EEG Derived Laterality Metrics as a Biomarker for of Upper Limb Recovery in Stroke

An Explorative Study into EEG Biomarkers for Longitudinal Stroke Recovery

By

G. C. Prins

in partial fulfillment of the requirements for the degree of

Master of Science
in Biomedical Engineering

at the Delft University of Technology,
to be defended publicly on Tuesday, August 31, 2021, at 09:30 AM.

Thesis Committee:	Prof. dr. F.C.T. van der Helm	TU Delft
	Ir. K. Rassels	TU Delft
	Ir. J. van der Cruijsen	TU Delft

TU Delft

Contents

Abstract

Problem: A biomarker that accurately predicts recovery of ischemic stroke for patients with poor baseline Fugl-Meyer Assessment of the Upper Extremity (FMA-UE) is lacking. Biomarkers that predict recovery while providing functional insight into the underlying neural process are highly desired for optimal clinical care.

Objectives: This explorative study aims to determine potential biomarkers from Somatosensory Evoked Potentials (SEP) using ElectroEncephaloGraphy (EEG).

Brain asymmetry metrics are derived from high-density EEG recordings of five longitudinal stroke patients during the first six months of stroke recovery. In addition, EEG sources and their interactions, constrained by anatomical information from (d)MRI, are explored for a potential biomarker.

Results: Subjects with low baseline FMA-UE show a trend of increased recovery as the Laterality Index (LI) of the infarcted hemisphere increases, although it is not significant within this small group. The LI of the non-infarcted hemisphere shows a significant trend of high LI values at baseline that decrease to lower values during recovery. This effect was tested on a different dataset of 17 longitudinal stroke patients (without dMRI data). The results in this second group showed strong variability between subjects and measurements. The non-infarcted hemisphere is able to significantly predict the FMA-UE for both datasets. On the other hand, estimated effects for the LI of the infarcted hemisphere did not show significant values. Biomarkers were not derived from EEG sources and their interactions.

Conclusion: In this study, we have demonstrated the potential of the LI as a biomarker for stroke recovery. Small sample size and absence of controls make hard clinical conclusions impossible. However, our findings show that the LI might predict recovery of the FMA-UE, even at low baseline FMA-UE. The LI of the non-infarcted hemisphere is able to significantly predict the FMA-UE of the affected hand, a surprising discovery that might be attributed to background cortical activity or ipsilateral SEP components. Derivations from EEG sources and their interactions might lead to more sensitive metrics and novel insights into stroke rehabilitation.

Significance: If the discovered trends apply to a larger sample size, asymmetry metrics from SEP's have prognostic value in stroke recovery.

Introduction

Background

Worldwide, stroke is the second most common cause of disability and mortality (Feigin et al., 2019). After a stroke, the outcome and degree of impairment depend primarily on the stroke severity and patient age (Oliveira-Filho & WJ, 2010). Current trends suggest that the global burden of stroke increases with the aging population (Feigin et al., 2015). In order to correctly treat the increasing number of stroke patients, a fundamental understanding of the mechanisms of stroke recovery is needed.

Many stroke patients suffer from hemiparesis, i.e., weakness or inability to move one side of the body. Clinical scores provide information on the degree of hemiparesis, with the Fugl Meyer Assessment (FMA) on the motor ability of stroke patients. The Erasmus Modified Nottingham Sensory Assessment (EMNSA) determines the sensory capabilities after stroke. The FMA at baseline can be used as a predictor for recovery six months post-stroke (Prabhakaran et al., 2008; Winters et al., 2015). However, the FMA as a predictor for recovery performs poorly when the FMA is low at the onset of stroke recovery (Saes et al., 2021). Clinical scores provide a basis for quantification of the current situation of the patient. However, clinical scores do not quantify the underlying neural process and provide limited functional insight into the underlying neural processes of stroke recovery. Therefore, there is a need for a biomarker that provides functional insight into stroke recovery, which could predict stroke recovery for patients with poor FMA at baseline.

Several parameters have been derived to predict motor recovery in stroke. Structural methods have indicated that corticospinal tract integrity is a predictor of stroke recovery (Lin et al., 2019). Other parameters that predict motor recovery have been derived from cortical activity. Saes and colleagues (Saes et al., 2021) determined brain asymmetry to predict motor recovery in stroke. Other research found that features derived from a cortical response to electrical stimuli could predict motor recovery after stroke (Kalogianni et al., 2018).

Detecting Brain Signals

Several imaging modalities and strategies can be used to quantify changes in brain activity during stroke recovery. ElectroEncephaloGraphy(EEG) can be used to measure brain signals. Despite the poor spatial resolution, EEG boasts a temporal resolution in the millisecond's range (O. G. Filatova et al., 2018). Taken together, this allows EEG to be an excellent method to study fast dynamics in the brain. EEG signals can be studied directly but can also be used for source localization, where the cortical sources are mapped from measured scalp EEG signals. However, the number of sources generally outnumbers the number of electrodes used for source localization. As such, source localization is an ill-posed problem, and correctly

identifying sources remains a key challenge in EEG research (Jatoi et al., 2014). Functional Magnetic Resonance Imaging (fMRI), a different imaging method, suffers from the opposite problem. fMRI provides excellent spatial resolution in the order of 3-4 mm, but even 500 microns or less can be reached (Glover, 2011). It is important to note that fMRI determines the location of the hemodynamic response resulting from brain activity instead of the location of the brain activity itself. However, this distance is generally less than 25 μm (Kim & Fukuda, 2008). The spatial resolution of fMRI allows viewing of source activity much more precisely compared to EEG. However, the peak of the hemodynamic response in fMRI is around 5-6s after stimulus, giving a much lower temporal resolution (Glover, 2011). This time resolution can be used to compare functional differences in the brain, but cannot discern the activity of quick neuronal processes in the order of milliseconds, which are a common target in neuroscientific research (O. G. Filatova et al., 2018).

Alternatively, anatomical imaging methods are used extensively in brain research (Owen et al., 2017; Soulard et al., 2020; Yeh et al., 2013). T1 MRI images can be used to view high-resolution anatomical images of the (lesioned) brain. Diffusion-weighted MRI (dMRI) is a variant of MRI imaging. dMRI can be used to infer white matter connections between brain regions (Owen et al., 2017). MRI and dMRI provide excellent high-resolution images but provide no insight into functional changes in the brain (Boyd et al., 2017).

The integrity of the somatosensory system has been a neglected area in predicting stroke recovery. However, somatosensory impairment is associated with stroke severity (Laaksonen et al., 2012). In a proof of principle study investigating the somatosensory system, Filatova and colleagues (O. G. Filatova et al., 2018) found the healthy brain to be highly lateral, i.e., most activity is confined to a single hemisphere. In contrast, hemiparetic individuals have been known to recruit the non-infarcted hemisphere during movement (Buma et al., 2010; Johansen-Berg et al., 2002). It is unclear if this translates to the somatosensory system. Research into the relationship between the somatosensory system and stroke found differences in laterality based on stroke severity after stimulating the sensory system using a wrist perturbation robot (Vlaar et al., 2017). In addition, increased inter-hemispheric connections were found in a study of source interactions in the somatosensory system (O. G. Filatova et al., 2018). These findings suggest that the somatosensory system's recruitment of the non-infarcted hemisphere is possible and should be investigated further.

Another way to stimulate the sensory system is by using the Somatosensory Evoked Potential (SEP) (Al-Rawi et al., 2009; Feys et al., 2000; Huang et al., 2004; Keren et al., 1993). A SEP is the brain’s response to an external stimulus. A SEP can be measured non-invasively using EEG or fMRI (Arthurs & Boniface, 2003; Kalogianni, Daffertshofer, et al., 2018; Schubert et al., 2008). After stimulation, several peaks can be detected in the measured EEG, such as the P20, P30, P50, or P100 peaks, where the number indicates the general latency of each peak. These peaks can be

found in electrodes near the sensorimotor cortex contralateral to the stimulated limb (Allison et al., 1989). Changed responses to electrical stimuli are associated with impairment, for example, a lower peak-to-peak amplitude was found for stroke subjects than healthy controls (Al-Rawi et al., 2009). Most SEP activity is found in the hemisphere contralateral to stimulation (Backes et al., 2000). Changes in SEP peaks or SEP-related activity in both hemispheres could indicate changes in asymmetry. For this reason, SEP-derived metrics can be used as a potential biomarker in stroke recovery.

Nowadays, it has become clear that combining several imaging modalities can complement each other. The thought is that the poor spatial resolution of EEG can be improved by using information from different imaging modalities. Source localization using a Wiener filter (Kajihara et al., 2004) or hierarchical Variational Bayesian (hVB) source estimation (Sato et al., 2004) complements source imaging using fMRI information. Ideally, not only the location of active sources would be determined, but causal relations between sources as well. Inferring relations between sources can be done using a directed form of functional connectivity, e.g., Granger causality, where statistical causality is inferred by determining whether one signal precedes another signal (Bastos & Schoffelen, 2016). However, Granger causality is based purely on signal properties and does not consider anatomical constraints (Bastos & Schoffelen, 2016). Other methods determine effective connectivity. These require an underlying model but can infer a more substantial degree of causality than just statistical causality (Bajaj et al., 2015). However, effective connectivity methods generally require prior assumptions on the model structure. Variational Bayesian Multimodal EncephaloGraphy (VBMEG) has been shown to infer effective connectivity with minimal assumptions on the model structure (Takeda et al., 2019). VBMEG estimates sources using an hVB source localization method. By combining located sources with anatomical information estimated from dMRI data, a MAR model is built to determine causal interactions between sources and infer information flow through the brain network (Fukushima et al., 2015; Takeda et al., 2019).

Earlier research has shown the potential of the VBMEG method on healthy participants (Fukushima et al., 2015; Takeda et al., 2019). Recently, an effort has been made to utilize the potential of VBMEG in investigating brain changes during a brain disease (O. G. Filatova et al., 2018) and showed the ability of VBMEG to detect changes in signal propagation in stroke patients.

Problem Statement

The problem is that a biomarker that predicts stroke recovery, especially at low FMA, is lacking. Accurate prediction of stroke recovery is essential to ensure optimal clinical care.

Research Goals

The goal of this study is to find potential biomarkers for stroke recovery from high-density EEG recording and EEG source interactions. Based on earlier studies (O. G. Filatova et al., 2018; Kalogianni et al., 2018), we hypothesize that a measure of brain asymmetry derived from SEP's could be a potential predictor for stroke recovery at baseline. Furthermore, biomarkers derived from EEG source interactions are expected to be more sensitive than metrics derived from EEG channel data. Metrics derived from EEG source interactions have separated activity of interest from noise, increasing the sensitivity.

In this explorative study, we have the following research goals:

- Quantify brain asymmetry of SEP's after an ischemic stroke using EEG and EEG source interactions
- Determine the ability of one of the found brain asymmetry metrics as a potential biomarker for motor recovery six months after ischemic stroke

We investigate quantification of asymmetry using EEG-derived metrics: SEP peak amplitudes and laterality index (LI) using EEG recording of five longitudinal stroke subjects. In addition, we intend to quantify the degree of asymmetry using the VBMEG method. We want to know if VBMEG is more sensitive compared to laterality measures derived from regular EEG data.

Methods

Subjects

Five acute ischemic stroke patients were included in this study. Mental capacity was confirmed using the Mini-Mental State Examination. Patients were recruited with informed consent and permission by the Medical Ethical Committee of the Amsterdam University Medical Center location Vrije Universiteit and the Reinier De Graaf Ziekenhuis board in Delft. Trial Protocol was registered on October 23, 2013 (identifier NL4084, NTR4221) and amended on April 4, 2016, to include longitudinal dMRI measurements (L. Filatova, 2019).

Inclusion criteria were: over 18 years of age, first-ever ischemic stroke in an area supplied by the anterior, medial, and/ or posteri-or cerebral arteries, Cerebro Vascular Accident (CVA) in the last five days, upper limb paresis as defined by NIHSS item 5a/b score>0, mini-mental state examination (MMSE) score of >19 (in case of lower score due to aphasia, an additional informed consent form was signed) and ability to sit without support. Exclusion criteria were: pre-existing pathological or neurological conditions, a pacemaker or other metallic implant, pre-existing orthopedic limitations of the upper limb, botulin-toxin injections or medication that might affect upper limb functionality in the past three months, and high epilepsy risk.

Eighteen patients were included in the study from November 30, 2016, to March 21, 2018. 12 Subjects dropped out of the study. One due to skin rash, one wrong stroke diagnosis, one death, two repeated strokes during the study, one claustrophobia, and six subjects were too burdened by study participation (L. Filatova, 2019) . For one subject, a significant amount of data was missing and was excluded. EEG acquisition was performed in a specialized van designed for EEG recordings at a location convenient for subjects. MRI and dMRI images were acquired at the Reinier de Graaf Ziekenhuis in Delft. Of the remaining subjects, all were aged between 43 and 74 (mean 62, std: 10), with five male participants.

Additional Dataset

An additional dataset was obtained containing 20 subjects. Subjects were recruited upon hospital admission under the same trial protocol and same exclusion criteria as described above. This data was used in prior research from the same research group (Kalogianni et al., 2018), as such it was already pre-processed. Two subjects were discarded from the pre-processed data due to a possible mismatch of dominant and affected arm, which could not be corrected without pre-processing the data again. One subject was discarded due to double data files without the possibility of identifying the correct data. Seventeen subjects remained.

Data Acquisition

Figure 1 displays the data acquisition schedule for all subjects. Subjects were exposed to four EEG and four (d)MRI measurements over six months. In Addition, Clinical testing was performed by a physician.

Clinical testing of the patients was performed from the subacute phase (within one week post-stroke) until the chronic stage (six months post-stroke). Clinical measures were taken during the first week, five weeks, twelve weeks and six months after stroke.

Affected upper extremity sensory impairment was measured using the EMNSA (Stolk-Hornsveld et al., 2006). In the sensory section of the EMNSA, the upper extremity is separated into four sections: the Upper Arm (UA), the Lower Arm (LA), the hand (H), and fingers (V). Each section is graded on its sensory ability. The sensory ability of a subject is graded on a scale from 0 to 40 points.

The motor capability was tested using the FMA-UE (Dunning, 2011). The FMA-UE is a test to determine motor recovery after stroke. The maximum score of the FMA-UE is 66, indicating an unimpaired participant.

Clinical testing was performed similarly for the additional dataset from earlier research (Kalogianni et al., 2018).

EEG Acquisition and Nerve Stimulation

EEG measurement was performed in a NEN1010 approved measurement van. Subjects were seated comfortably with their hand resting on their lap. The Median nerve of both arms was stimulated on the wrist. Patients were fitted with a stimulator

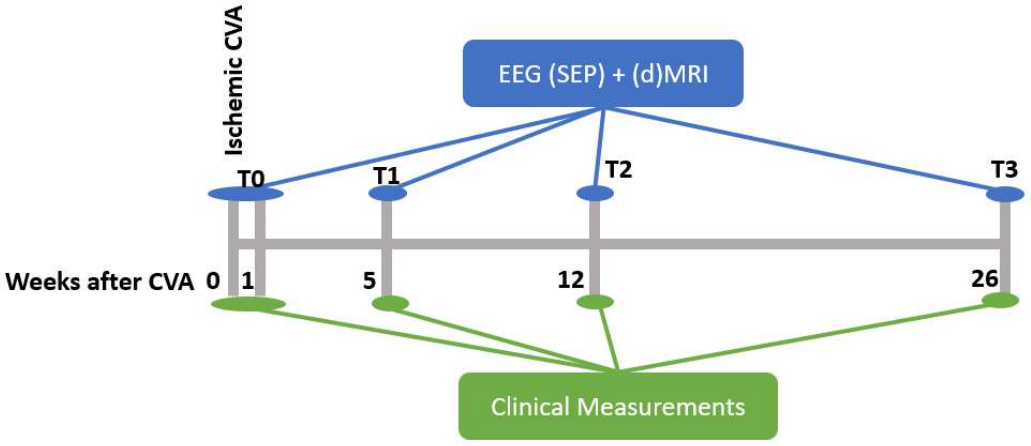

Figure 1 Data Acquisition schedule. The first EEG and (d)MRI data were acquired in the first week after stroke onset. Additional data acquisition was performed five weeks, twelve weeks, and six months after stroke onset. Clinical scores were obtained in the first week after stroke onset. Later clinical scores were obtained five weeks, twelve weeks, and six months after stroke onset.

band. After the median nerve was located, patients were stimulated with increasing amplitude until a thumb twitch was displayed without inflicting pain or discomfort. Stimulation was performed for 500 trials for each hand. EEG was recorded using a 62 channel EEG amplifier and a cap arranged according to a subset of the extended 10/20 system (TMSi, Netherlands).

The ground electrode was set to the left mastoid and the sampling rate was 2048 Hz. Besides antialiasing filters, no filters were applied online. Electrode and fiducial points were measured using ANT Neuro Xensor (ANT Neuro, Enschede). The average time between EEG setup and finishing finger stimulation was around 60-90 min including setup and initial resting-state measurements. This length of experimental time is short enough not to be too great of a burden on stroke patients without mental defects (O. G. Filatova et al., 2018).

EEG acquisition of the additional dataset was acquired using the exact same setup and is further described in the Kalogianni's dissertation (Kalogianni, Saes, et al., 2018).

EEG Pre-Processing

Figure 2 displays the flowchart of EEG-preprocessing. All EEG data were processed using EEGlab (Delorme & Makeig, 2004) and Fieldtrip (Oostenveld et al., 2011), both are open-source toolboxes for MATLAB. The stimulation artifact was removed by a -10 to 10 ms blanking window around stimulation and interpolated using a third-order auto-regressive model. The data were downsampled to 512 Hz. Continuous EEG data was notch filtered around 50 Hz to remove line noise. A bandpass filter between 1 and 100 Hz was applied to remove low-frequency drift and high-frequency content. Noisy channels were removed manually. Epochs were extracted with a window of -50 to 200 ms around stimulation. After epoch extraction, epochs with significant artifacts (e.g., movement artifacts) were discarded manually. Independent Component Analysis (ICA) (Delorme & Makeig, 2004) was used to remove components of eye blinks, movements, or other sources of artifacts. EEGLAB's

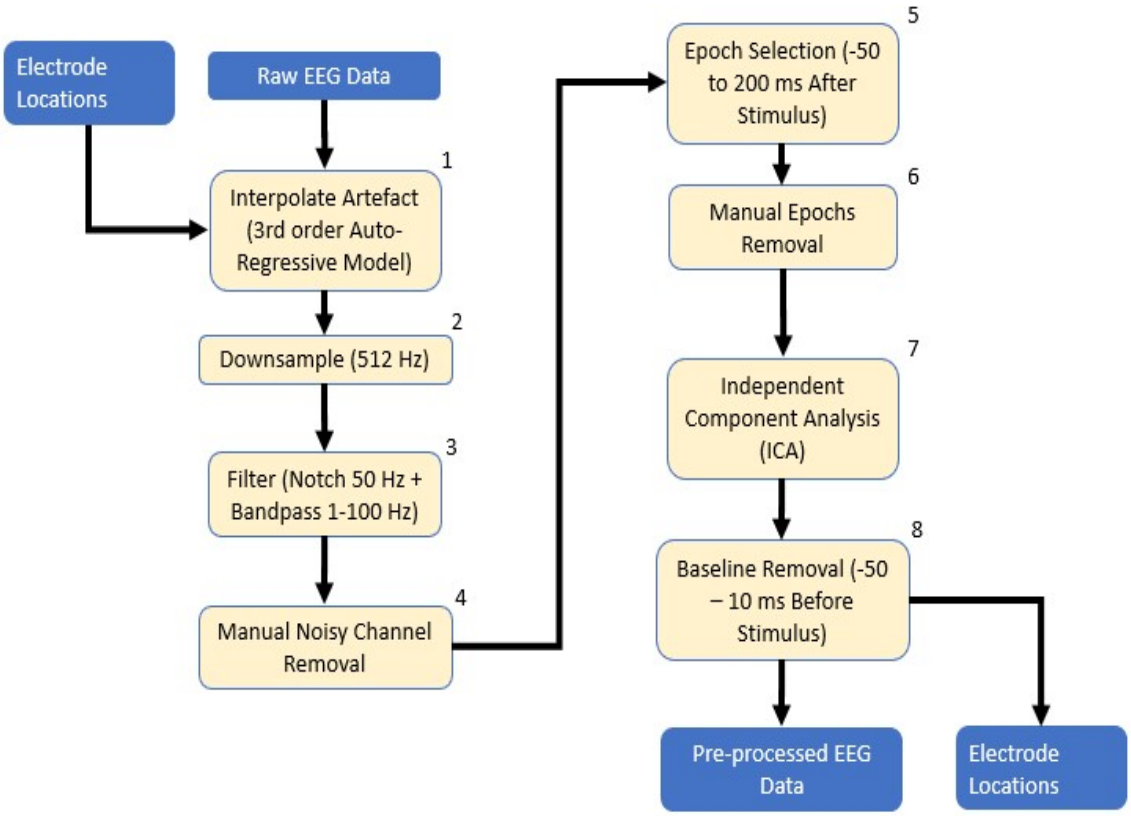

Figure 2 Flowchart of EEG Pre-processing. The stimulation artifact is removed using a third-order auto-regressive filter (1). Data were downsampled to 512 Hz (2). Data were filtered with a 1-100 Hz bandpass filter to remove high-frequency content and low-frequency drift. A 50 Hz notch filter was applied to remove line noise (3). Noisy channels were removed manually through visual inspection (4). Epochs were extracted using a window of – 50 to 200 ms after stimulus (5). Epochs with muscle artifacts were selected and removed manually (6). ICA was performed, and eye and muscle components were removed (7). The baseline from -50 to -10 ms with respect to the stimulus was removed(8). Pre-processed EEG data and electrode locations were extracted for further analysis.

IClabel labeled all components. Components with at least 90% certainty from IClabel for muscle artifacts and 70% certainty for eye artifacts were automatically marked for removal. All components were checked manually, remaining eye, muscle, or interpolation components were removed manually. If a component contained both artifact and brain elements, components were given the benefit of the doubt.

After component removal, baseline correction was applied from 50 ms to 10 ms before stimulus onset.

EEG data from the additional dataset were pre-processed as described in earlier research by Kalogianni and colleagues (Kalogianni, Saes, et al., 2018). EEG data were using Matlab, Fieldtrip (Oostenveld et al., 2011) and EEGlab (Delorme & Makeig, 2004). The stimulation artifacts were removed by linear interpolation until 6

ms after stimulus onset. Data were bandpass filtered between 1 and 250 Hz using a bi-directional fourth-order Butterworth filter. Data were segmented into epochs lasting from 50 ms before stimulus to 200 ms after stimulus. Noisy epoch and channels were removed manually. Generally, around 400 trials remained after removal and around 50 channels. Data were re-referenced to the common average, and SEP's were created by averaging over all trials. After processing, a SEP for each patient for the infarcted hemisphere and a SEP for the non-infarcted hemisphere remained.

(d)MRI Acquisition

Image acquisition was performed with a 3T MRI scanner (Philips Achieva, Philips Healthcare, Best, The Netherlands). Anatomical T1 MRI imaging had the following settings: TE = 20 ms, TR = 2000 ms, Flip Angle = 90°, imaging matrix 512x512 for 26 slices. The dMRI acquisition protocol had 40 non-collinear gradient directions uniformly sampled over a sphere for each of two b-values, 1000 and 2000 s/mm2. dMRI data for both b values were acquired in a single scan. dMRI settings were: TE=100 ms, TR= 6506 ms, imaging matrix = 96x96, 50 consecutive slices, thickness of 2.5 mm, and slice spacing 2.5 mm. One image for each acquisition had no diffusion weighting with a b value of b=0 s/mm2.

EEG Analysis

The Signal to Noise Ratio (SNR) was calculated for all EEG measurements. The SNR was calculated for each electrode by dividing the signal power with the signal variance, similar to previous studies (Vlaar et al., 2017). A notable difference is that Vlaar calculated the SNR in the frequency domain, while the SNR was calculated in the time domain in this study.

The SNR was defined as dividing the average response by the variance across recorded periods (Vlaar et al., 2017)

$$SNR = \frac{\hat{E}}{\sigma^2} = \frac{\Sigma_{k=1}^{N} \hat{x}(k)^2}{\Sigma_{k=1}^{N} \frac{1}{P-1} \Sigma_{P=1}^{P} \left(x^{[p]}(k) - \hat{x}(k)\right)^2} \quad (1)$$

where $\boldsymbol{x}$ is the recorded signal from an electrode, $\hat{\boldsymbol{x}}$ is the average response. $\boldsymbol{N}$ is the number of samples in one trial, $\boldsymbol{k}$ is a sample in a period $\boldsymbol{p}$, and $\boldsymbol{P}$ is the total number of periods.

After pre-processing, it is expected that most of the sources of variance in the measured signal are from cortical background activity.

After calculating the SNR, SEP's were calculated by averaging the remaining trials, resulting in a SEP for the infarcted and non-infarcted hemispheres. P20, P30, and P50 components were identified based on their latency and a butterfly plot of all channels. The P20 peak was identified from 19 to 25 ms, P30 25 to 38 ms, P50 45 to

60 ms, and P100 from 90 to 115 ms. The time intervals for peak detection were extended to account for increased latency due to stroke (Julkunen et al., 2005).

We identified the channel with the highest peak within the time window and an above-average SNR for each peak and every SEP measurement. The channels ERP was plotted and peaks were validated through visual inspection. In addition, the SEP peaks were accepted only when a dipole pattern (validated through a topological distribution) was present. Whenever this was not the case, the amplitude was marked as non-identifiable and set to 0.

Laterality Index

From the SNR, the LI was calculated. Electrodes located above the sensorimotor cortices were separated into two sets. The left side included odd EEG electrodes above the sensorimotor cortices named F1, F3, F5, FC1, FC3, FC5, C1, C3, C5, CP1, CP3, CP5, P1, P3, and P5. The right side included even EEG electrodes above the sensorimotor cortices named F2, F4, F6, FC2, FC4, FC6, C2, C4, C6, CP2, CP4, CP6, P2, P4, and P6. The sets are referred to as the ipsilateral (same side) with respect to the stimulated limb and contralateral (other side) with respect to the stimulated limb. The SNR was averaged for all electrodes in each set. These sets were used to calculate the laterality index similar to other research (Vlaar et al., 2017):

$$LI = \frac{SNR_{contra} - SNR_{ipsi}}{SNR_{contra} + SNR_{ipsi}} \quad (2)$$

The LI calculated in this manner is obtained similar to LI's from other studies using fMRI (Pujol et al., 1999) or EEG (Jung et al., 2003; Vlaar et al., 2017). The LI is bounded between -1 and 1, 1 indicates all activity is present on the contralateral (stimulated) side and -1 indicates all activity on the ipsilateral (non-stimulated) side. An LI calculated from stimulation of the affected hand will be referred to as the LI of the infarcted hemisphere. An LI calculated from stimulation of the unaffected hand will be referred to as the LI of the non-infarcted hemisphere.

Statistical Analysis

A linear mixed effect model was fitted on the LI and FMA-UE. The model was structured to determine whether the LI could predict the FMA-UE with a random slope and intercept for each patient. The model was fitted using MATLAB's fitlme (MathWorks, Natick, USA). The distribution of residuals was checked using a QQ-plot and histogram of residuals.

Connectome Dynamics Estimation

The following section explained the methodology of connectome dynamics estimation using VBMEG. In this study, connectome dynamics were not estimated.

VBMEG

The VBMEG method consists of source localization and estimation of dynamic information flow from one source to another. The VBMEG toolbox combines source localization with anatomical dMRI data to provide a more accurate model to calculate dynamic information flow.

Figure 3 displays the pipeline of the VBMEG toolbox. T1 MRI images are processed to create a cortical model and a head model. The leadfield matrix is built from EEG electrode locations, the head model and the cortical model. Combined with pre-

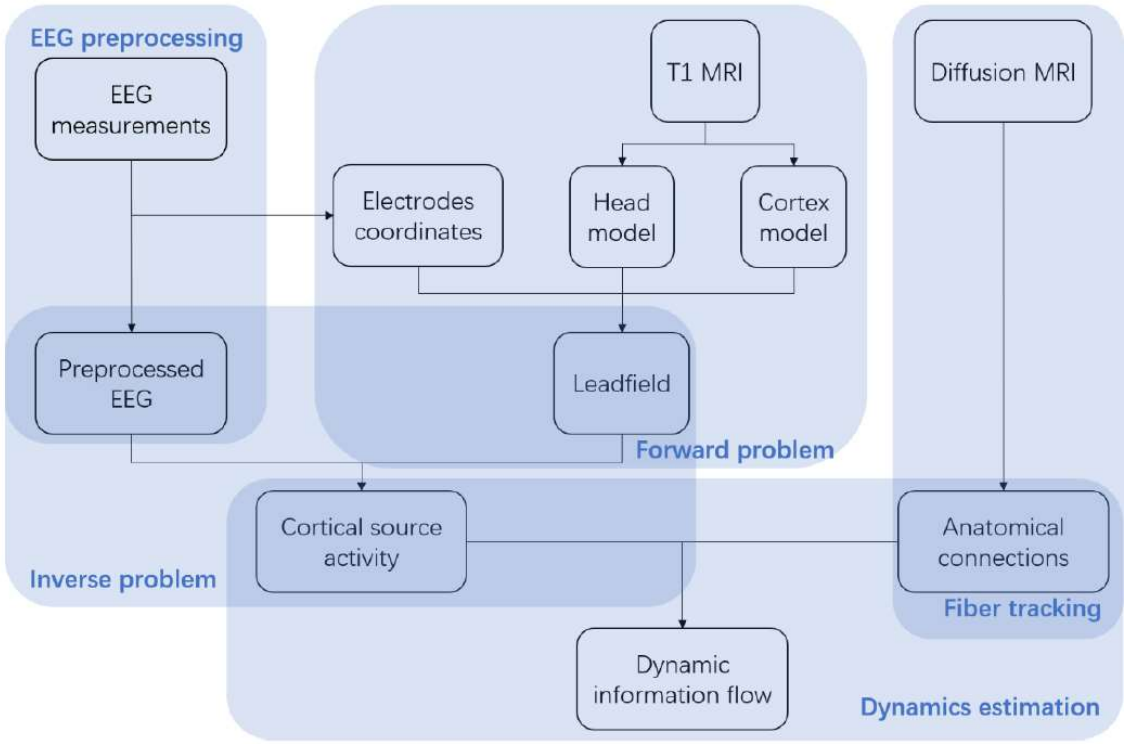

Figure 3 overview of VBMEG pipeline. EEG is pre-processed as described above. T1 MRI images are processed to create a 3-shell head model and a cortical model. Together with electrode coordinates from EEG data leadfield matrix is created. This step is the Forward problem in source localization. The inverse problem is solved using the hVB approach to estimate cortical source activity. Fiber tracking is performed on diffusion MRI data. Anatomical connections obtain from fiber tracking are combined with cortical source activity to estimate dynamic information flow between sources. Figure obtain from: O. G. Filatova et al., 2018

processed EEG data, source activities are estimated using the hierarchial Variational Bayesian (hVB) method (Sato et al., 2004). Unlike the original work by Sato, our dataset did not contain functional MRI data for source localization.

dMRI data is pre-processed, and fiber tracking is performed. By combining anatomical connections obtained by fiber tracking with source activity from source localization, a Multivariate Autoregressive (MAR) Model is built.

Source Localization

Source localization can be separated into the forward problem and the inverse problem, see Figure 3. The forward problem is estimating the potential distribution for known source(s) and the known head model. In the inverse problem, sources are estimated from measured potentials. The inverse problem is ill-posed as the number

A cortical model was created for each subject from the T1 MRI image using Freesurfer, an MRI processing software (Dale et al., 1999; Fischl et al., 2002, 2004; Fischl, Sereno, & Dale, 1999; Fischl, Sereno, Tootell, et al., 1999; Fischl & Dale, 2000). Freesurfer extracted the inner skull and outer scalp surface. In addition, a polygon model was constructed of the cortical surface. A three-shell head model (CSF, Scalp, Skull) was built using the Boundary Element Method (BEM) from the VBMEG Toolbox (Fukushima et al., 2015). Ten thousand vertices on the cortical surface were selected as possible dipole sources. From the dipole sources, electrode positions, and the 3-shell head model, the leadfield matrix was calculated. Standard conductivity settings from the VBMEG toolbox were used (CSF = 0.62 S/m, skull = 0.03 S/m, scalp = 0.62 S/m) (ATR Neural Information Analysis Labs, 2018).

All subjects have small lesions in the brain. All but one subject had small lesions located deep in the brain. Two lesions were too small for CT representation. One patient suffered from small lesions in the frontal and parieto-occipital lobes. Although of small size, the lesion is located close enough to the surface to be situated between a potential source and electrode. Previous research has indicated that lesions can lead to significant errors in source localization(Vatta et al., 2002, 2001), especially when the lesion is between source and electrode (Vatta et al., 2000). Care should be taken in this patient's case to ensure the lesion does not affect source localization.

The hVB method is similar to the Minimum Norm Estimate (MNE) or Wiener filter. All these methods use a regularization term to solve the inverse problem. The MNE solution uses an identity regularization term (Sato et al., 2004). The Wiener filter is a step more complicated and uses the current variance obtained from fMRI data to regulate the least-squares calculation (Kajihara et al., 2004; Sato et al., 2004). Similar to the Wiener filter, the hVB method uses the current variance to calculate the regularization term. However, the current variance is defined as an unknown parameter and estimated iteratively (Sato et al., 2004).

Iterative estimation of the current variance is performed by the hierarchial Variational Bayesian method, a variant of the Variational Bayesian method using a hierarchical prior.

A hierarchical prior places a softer constraint on the variance compared to using a normal prior(Sato et al., 2004). Estimating the current variance is constrained further by a smoothness constraint, ensuring correlated activity between neighboring sources. Prior information on the current variance is obtained from EEG and/or fMRI data. The current variance is estimated iteratively (Sato et al., 2004). The soft constraint on the current variance makes the hVB method is more robust to poor fMRI data.

Fiber Tracking

Fiber tracking was used to infer anatomical connections between regions of interest from dMRI data. Before fiber tracking, the cortical surface model was parcellated into 250 parcels distributed equally over the cortical surface. MRTRix 0.2.13 was used to perform fiber tracking for all parcels, i.e., fiber tracking was used to determine anatomical connections of each parcel to all other parcels.

The number of parcels is a parameter that can be chosen by the user and determines the number of variables in the MAR model. A small amount of parcels leads to parcels of large size where a single parcel may contain the activity of multiple sources. A larger number of parcels increases the resolution and decreases the chance of a single parcel spanning multiple sources. However, the computation time of fiber tracking increases quadratically with the number of parcels, leading to heavy computational requirements.

MAR model estimation

A MAR model was used to estimate the dynamic information flow to determine causal relations between sources. Source activity was clustered into the parcels created during fiber tracking. The source activity within each parcel was calculated as the mean contained dipole moments. The MAR model was constrained using the output from fiber tracking, making sure only anatomically connected parcels have nonzero weights (See appendix A, section Mar Model). Time lags in the model were estimated based on the theoretical conduction velocity of axons equal to 6 m/s (Fukushima et al., 2015). Only the terms with specific time-lags were included in the model. The order for inter-variable interaction is one (O. G. Filatova et al., 2018). In this setup, the model can be represented by a 2D -matrix for inter-source dynamics. Intra-source dynamics were set as second-order interactions. The MAR weights were estimated using an L_2 regularized least-squares method, constrained by fiber connections and time-lags.

Model Evaluation

The model was evaluated similarly to prior research using VBMEG (O. G. Filatova et al., 2018). Source localization and model accuracy were evaluated using Variance

Accounted For (VAF) (Kalogianni et al., 2018; Vlaar et al., 2017). Source localization was validated using an estimated EEG signal ($\widehat{\boldsymbol{M}} = \boldsymbol{L}\widehat{\boldsymbol{S}}$) generated from the estimated sources. The estimated signal is compared to the measured EEG signal ***M*** and the ***VAF*** is calculated as (O. G. Filatova et al., 2018):

$$\boldsymbol{VAF_{Mi}} = \left(\mathbf{1} - \frac{\boldsymbol{var}\left(\boldsymbol{M_i} - \widehat{\boldsymbol{M}}_{\boldsymbol{i}}\right)}{\boldsymbol{var}(\boldsymbol{M_i})}\right) \cdot \mathbf{100}\% \qquad (3)$$

Where ***i*** indicates the ith electrode. The dynamic information flow was validated using the MAR model. The source activity of the following data point (2 ms later) was estimated using the MAR model. The resulting source activity was compared to source localization results, leading to the following equation (O. G. Filatova et al., 2018):

$$\boldsymbol{VAF_S(t)} = \left(\mathbf{1} - \frac{\boldsymbol{var}\left(\boldsymbol{S(t)} - \widehat{\boldsymbol{S}}\boldsymbol{(t)}\right)}{\boldsymbol{var}(\boldsymbol{S(t)})}\right) \cdot \mathbf{100}\% \qquad (4)$$

Where ***S*** is a vector containing source activity from source localization, $\widehat{\boldsymbol{S}}$ is a vector containing the source activity estimated from the MAR model. The ***VAF$_S$(t)*** can then be calculated for every time point.

Results

Figure 4 A shows the sensory scores for all subjects over time. Almost all subjects score high on EMNSA scores from the onset except for one patient, and all score near-maximal scores from week five onwards. Figure 4 B shows the FMA-UE scores over the period of 6 months of recovery. Except for one patient, almost all patients recovered to almost the maximum score over six months.

SEP and Topographical Results

Figure 5 A shows the SEP results for two patients in the first week and the last week. In line with the literature (Desmedt & Cheron, 1980; Druschky et al., 2003; O. G. Filatova et al., 2018), the SEP shows a negative peak around 20 ms (P20), a positive peak around 30 ms (P30), and another positive peak around 50 ms (P50). A positive or negative peak can be identified around 100 ms, but this peak was less consistent among trials. Generally, the channel that displayed the highest SNR was located near the sensorimotor cortex (C3, C4, CP3 or CP4). However, this was not the case for all SEP recordings. Differences between subjects can be seen, which may be related to the lesion, differences between subjects, or variations of electrode location. Figure 5 B shows a topographic plot of SNR in the first week for a single subject, the same subject displayed in the top SEP plot of figure 5 A. For every electrode, the average SNR is displayed in a heatmap indicating locations activity. Left indicates the SNR for stimulation of the non-infarcted hemisphere. The right side

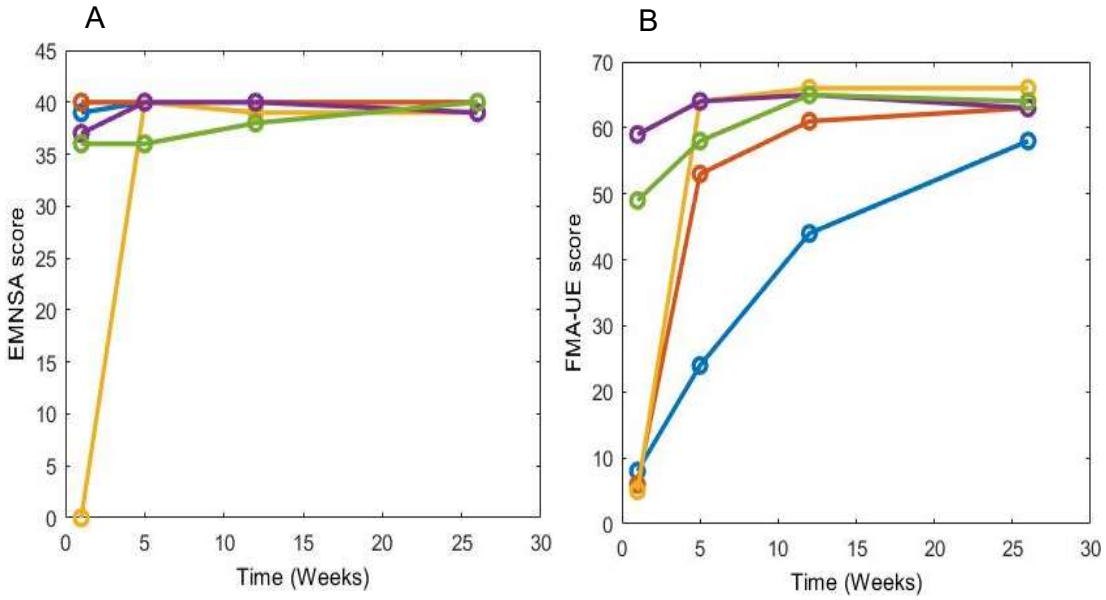

Figure 4 A: Clinical scores of the EMNSA over 26 weeks. Except for one patient, all EMNSA scores are nearly maximum at stroke onset. B: FMA-UE scores over time for each patient

displays stimulation of the infarcted hemisphere. In general, both topographic plots display the largest SNR in the sensorimotor cortex regions. However, the infarcted side shows a lower SNR in general, more frontal activity, and more background activity relative to activity near the sensorimotor cortex.

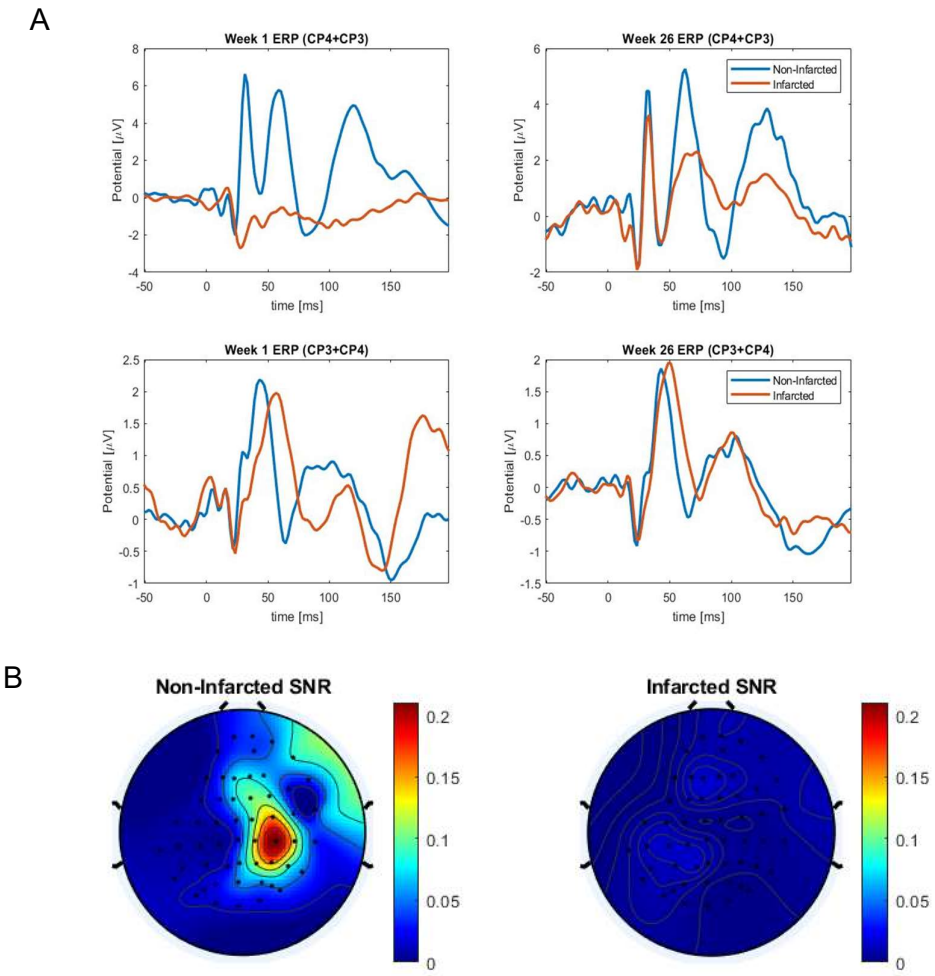

Figure 5 A: ERP at week 1 (left) and week 26 (right) of two patients for both the infarcted and non-infarcted hemispheres. The top row shows a subject with an initial EMNSA score of 0 that fully recovered. The bottom subject had a maximum EMNSA score initially. Both subjects scored low FMA-UE scores but recovered to almost the maximum score in the last week. 5 B shows the average SNR of each electrode plotted in a heatmap for the non-infarcted hemisphere(left) and the affected hemisphere (right) of the SEP displayed in the top left corner of figure 5 A. The non-infarcted hemisphere displays a much higher SNR and more laterality compared to the infarcted hemisphere.

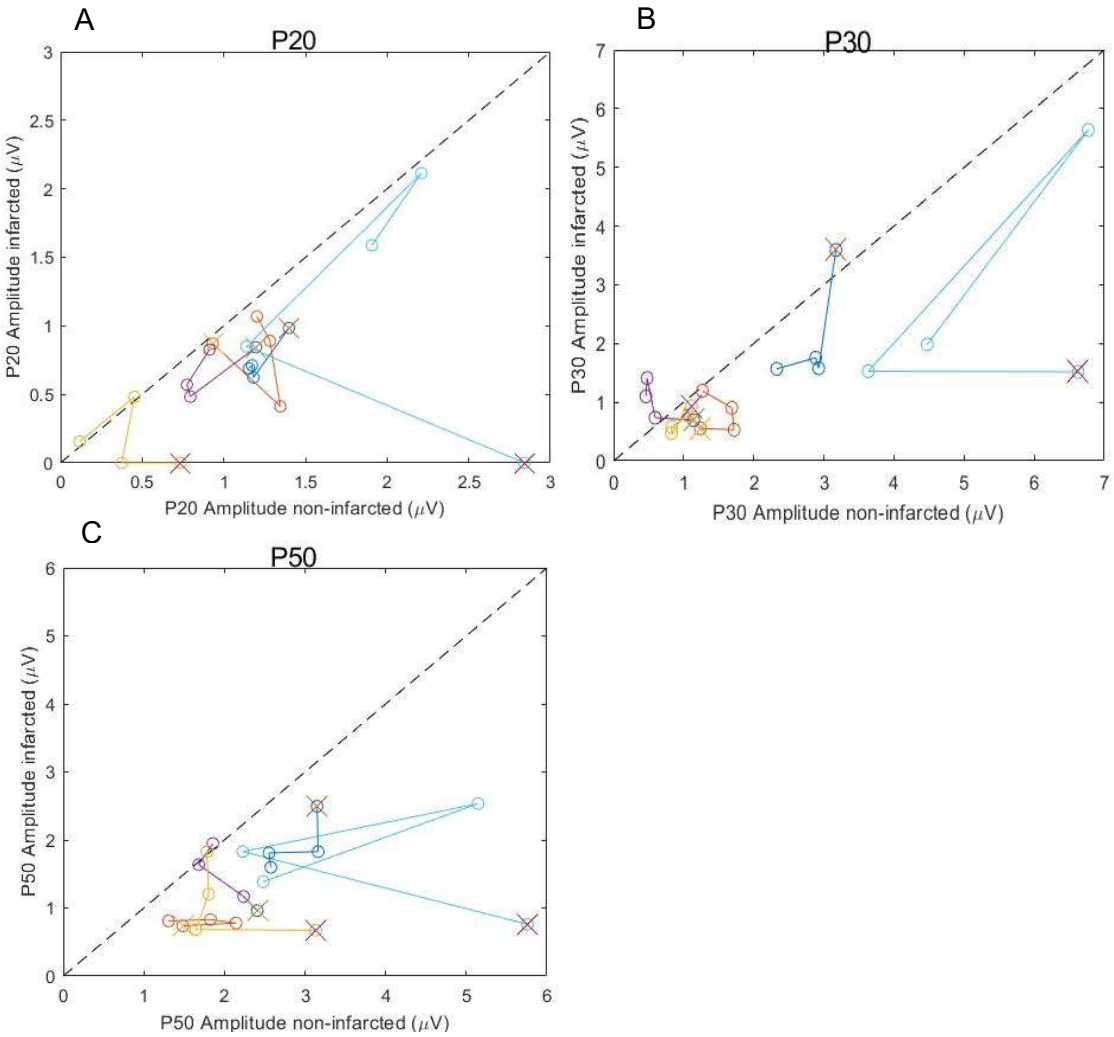

Figure 6. Amplitude plots of 3 SEP peaks for the infarcted hemisphere vs. the non-infarcted hemisphere. (A) shows the amplitude plots of the P20 peak. If no peak was found, the amplitude was set to 0. (B) displays the P30 peak, and (B) displays the P50 Peak.

Amplitudes

Figure 6 displays the amplitude of all subjects across all measurements for the P20, P30, and P50 peaks. If no peak could be found, the amplitude was set to 0. The P100 peak could not be detected in a large number of measurements and is not plotted. In general, SEP amplitudes of the infarcted hemisphere were of smaller amplitude in almost all measurements. All subjects show variation in SEP amplitude over measurements.

Laterality

Figure 7 A shows the LI plotted vs. the FMA-UE score for all patients for the infarcted hemisphere (A) and non-infarcted hemisphere (B). Both figures indicate variations for all subjects around an FMA-UE score of 60. In general, the LI of the infarcted hemisphere was lower than the LI of the non-infarcted hemisphere. Figure 7 B displays three subjects with low FMA-UE at baseline that recover towards near-

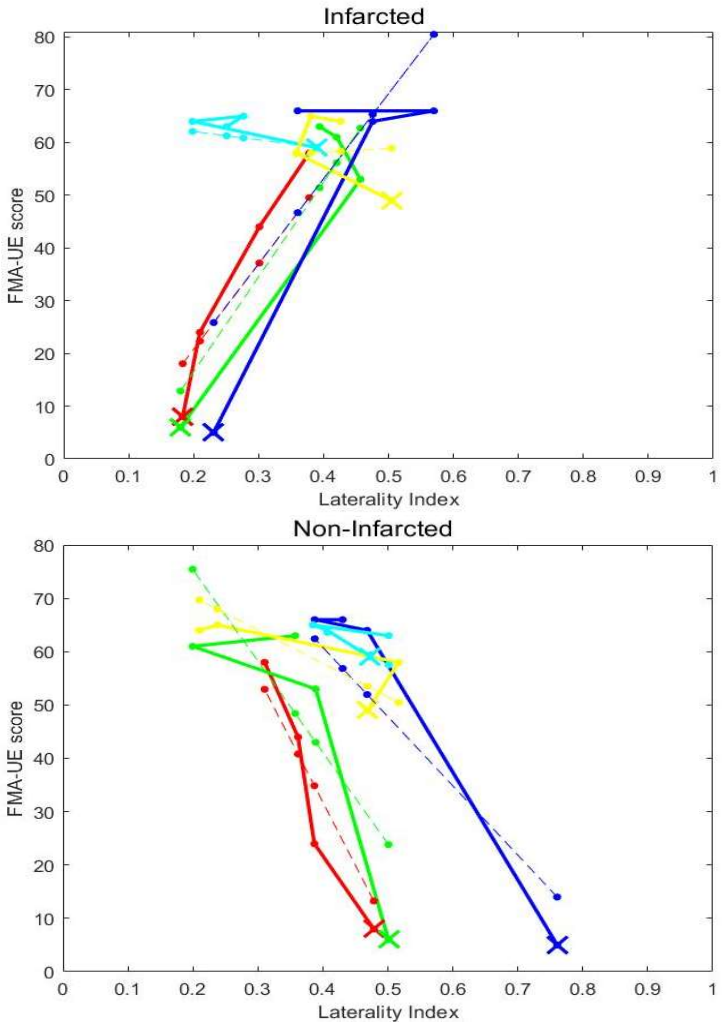

Figure 7 Laterality index vs. FMA-UE. The top figure displays the FMA-UE score vs. the LI for the infarcted hemisphere. Each line represents a subject with five lines or subjects in total. The bottom graph displays the FMA-UE vs. LI scores for the infarcted hemisphere. The dashed lines display the estimated models.

maximum FMA-UE values after six months. These three subjects display a trend of increased FMA-UE as the LI increases. Two other subjects have a higher FMA-UE at baseline and recover to near maximum FMA-UE after six months; these subjects display an opposite trend. The LI at baseline is higher and decreases as the FMA-UE increases.

The linear mixed effect model found an estimated slope of 98.88 (Confidence Interval (CI): [-3.379 201.1], p = 0.0572) adjusted R^2 = 0.7635. Non-infarcted had an estimated slope of -132.9 (CI: [-219.9 -45.86], p= 0.00487) adjusted R^2 = 0.7853.

Additional Dataset

The analysis of LI was reperformed on a different dataset of stroke patients. Figure 8 displays the LI vs. FMA-UE results of the additional dataset. Every line indicates a

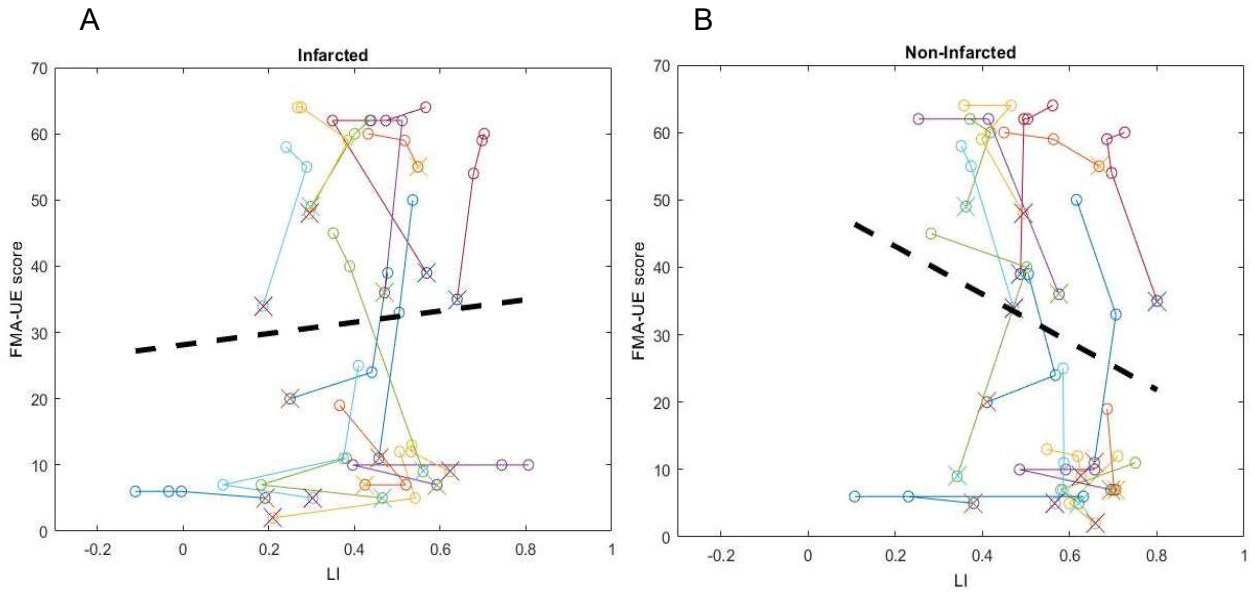

Figure 8 displays the FMA-UE vs. the LI of the additional dataset. Figure 8 A graph displays the infarcted hemisphere, and the non-infarcted hemisphere is displayed in figure 8 B. Each line represents a subject (17 in total). The first measurement is marked with an X. The dashed black line shows the average estimated linear model.

single patient, and the first measurement is marked with an X. The average trend determined over all patients is plotted with a dashed line.

The Infarcted hemisphere linear mixed model had an estimated slope of 8.510 (CI: [-18.57 35.59], p = 0.531) adjusted R^2 0.8413. The non-infarcted hemisphere had a estimated slope of 35.47 (CI: [-70.47 -0.4721], p = 0.0470) adjusted R^2 = 0.8626.

Discussion

We explored potential biomarkers for stroke recovery derived from SEP's using EEG channel data and VBMEG. Potential biomarkers were derived from SEP peaks or a laterality measure derived from EEG electrode data. A potential biomarker was not derived from VBMEG measurements since did not permit all processing. We investigated changes in brain asymmetry derived from SEP's from the first week to six months post-stroke. Due to the small sample size of five patients, hard clinical conclusions cannot be made, but we can comment on found effects and the reliability of the measurement method.

The clinical scores suggest that the research protocol was biased towards stroke patients with a good prognosis. Data acquisition was cumbersome for stroke patients, with four measurements of EEG and dMRI data in addition to clinical measurements. As a result, heavily impaired stroke patients are likely to drop out. The quick recovery of all subjects to high EMNSA scores supports this notion. Future research should strive to include stroke patients with poor prognoses by designing less cumbersome research protocols.

Scalp topography maps of the SNR showed the SEP response to be found in the sensorimotor areas. These findings are in line with literature (Allison et al., 1989; Spiegel et al., 1999). Scalp topographies showed little regarding activation of the non-infarcted hemisphere during SEP of the affected hand. Earlier research showed increased activation of the non-infarcted hemisphere (O. G. Filatova et al., 2018), but we could not show this using Scalp topographies of EEG electrode data.

SEP peak amplitudes were quantified and explored as a biomarker. The P100 peak was unidentifiable in a significant portion of the measurements and deemed unreliable. The SEP peaks show considerable variance in both the infarcted hemisphere and the non-infarcted hemisphere. This finding is in line with previous studies comparing SEP peak amplitudes of stroke patients (Kalogianni et al., 2018). The ability to adequately detect SEP peaks varied for each subject and measurement. Due to the large degree of amplitude variability and difficulty identifying several peaks, SEP peak amplitude was discarded as a potential biomarker for a dataset of this sample size.

EEG Derived Predictions Using the LI

Different trends in recovery were observed in subjects for the infarcted LI and FMA-UE and might be attributed to differences between stroke patients. Stroke recovery varies for each patient depending on severity and stroke location (Shelton & Reding, 2001). The differences between stroke subjects could be larger than the measured effect. Unless a larger dataset is used, statistically proving an effect for all stroke subjects might prove challenging. This different trend for subjects with high baseline FMA-UE might also be attributed to ceiling effects of the FMA-UE, which is capped

at a score of 66. For three subjects with low baseline FMA-UE, the LI shows potential to predict the FMA-UE. Our data did not include subjects with low baseline FMA-UE and poor recovery. Whether subjects with poor stroke recovery show a similar trend would be of interest. We hypothesize that subjects with poor recovery do not increase LI during recovery but recruit the non-infarcted hemisphere. Such subjects might display an opposite trend at the FMA-UE baseline. Changes in LI have to be determined for both recovering and non-recovering stroke subjects because differences are required for the LI as a predictor for recovery.

The LI of the non-infarcted hemisphere was found to predict the FMA-UE of the affected limb significantly. The decreasing trend was an unexpected result as we hypothesized the LI of the non-infarcted hemisphere to be unaffected by stroke. Previous studies of the somatosensory system (Vlaar et al., 2017) found values of the LI of healthy controls in a range of 0.1-0.5, similar to our values six months after stroke. It is important to note that this was during wrist perturbation instead of median nerve stimulation.

We have some theories on this surprising finding. We find it most convincing that the change in LI in the non-infarcted hemisphere can be attributed to a change in SNR in the infarcted hemisphere. This change in activity can be attributed to ipsilateral components of the SEP or background cortical activity. Previous research has found ipsilateral components of SEP's (Kakigi, 1986; Nihashi et al., 2005; Noachtar et al., 1997; Sutherland & Tang, 2006), although Kakigi attributed the generation of the components to the contralateral hemisphere. If such ipsilateral SEP components are present in the healthy brain, they are probably decreased after stroke. In line with this hypothesis, the observed trend in the non-infarcted hemisphere can be attributed to the recovery of ipsilateral components of the SEP. Another explanation can be found in the remaining background activity. It is assumed that background cortical activity is removed by averaging the SEP response over all trials during pre-processing. However, if pre-processing is unsuccessful in eliminating background activity, it could show up in the SNR of the non-stimulated hemisphere. After stroke, this background activity is decreased in the infarcted hemisphere and increases as the patient recovers, explaining our detected trend. More trials, different component selection strategies, or further processing such as source localization could remove more background activity and lead to more accurate results. If this hypothesis is true, removing all background activity should remove the observed trend. However, without measurements of healthy controls, the LI of median SEP's in a healthy subject is unknown. Whether the decreasing trend in the non-infarcted LI is a return to an LI comparable to healthy subjects or a different state cannot be concluded. And with such a small sample size, the found affect might be attributed to coincidence. Further processing steps should separate more irrelevant brain activity and give a better understanding on the origin of this trend.

The LI was calculated again on a separate dataset of longitudinal EEG data to determine if the detected trends could be observed in a different dataset. Compared

to the initial dataset, the LI of the additional dataset displayed a larger degree of variability in LI in both the infarcted and non-infarcted hemispheres. Observed trends in the initial dataset could not adequately be described to data in the additional dataset. Although the effect for the non-infarcted hemisphere was significant, we find the confidence interval too close to 0 for the trend to be considered reliable. A possible explanation could be different data pre-processing. The additional dataset was filtered between 1 and 250 Hz instead of 1 – 100 Hz. The stimulation artifact was interpolated differently, and no ICA was performed. Removing artifacts from eye movement or muscle using ICA decreases the dataset's variance, resulting in a higher SNR. Especially in measurements where the SEP response is small due to the stroke, a more considerable contribution from noise could lead to fluctuations in SNR and, consequently, the LI. ICA could aid in decreasing these fluctuations. In the obtained additional dataset, several indications were found for reasonable doubt on the cleanliness of the data, such as a possible mismatch in affected and unaffected hand stimulation. As described in the method section, these were excluded. However, a thorough visual inspection of all data could discover other similar data errors. Ideally, the additional dataset should be pre-processed again with ICA included and inspected visually to ensure reliable outcomes.

The laterality index provides quantification into the distribution of brain activity in individuals. Only relevant electrodes are incorporated into LI calculation. The LI is a global measure spanning multiple electrodes and time points. For this reason, it is more robust to sources of error from various irregularities compared to SEP peak data. In our data, we found considerable variance between and within-subjects for SEP peaks. For example, in figure 5 A, the bottom SEP displays a single or overlapping peak for P20 and P30. Other electrodes show these peaks separately. When calculating peak amplitude and latency, one must take reasonable care to ensure the correct electrodes are selected that show a peak and a maximum amplitude for ideal comparison between measurements. Although steps were taken to ensure correct results, this remains a possible source of error. A global measure that spans multiple electrodes is much less prone to errors from overlapping peaks or irregularities in latency. Furthermore, the LI is bounded between -1 and 1 and is an easy to interpret quantification of laterality. Taken together, the LI is an easy to interpret metric that can display a SEP response, even when SEP peaks are difficult to identify.

The LI is calculated from the SNR of the electrodes located above the sensorimotor cortex. This research is most interested in the SEP at low FMA-UE, where the SEP response is strongly affected by stroke. In the case of a SEP response strongly affected due to stroke, the SNR is poor. The noise contribution to the LI of this subject is more significant than measurements with high SNR and these measurements could suffer from fluctuations due to noise. The non-infarcted hemisphere does not suffer from this problem, as the SEP of the non-infarcted hemisphere can be detected in all measurements. The extra robustness to poor SNR

might partly explain the significance of the non-infarcted hemisphere in the regression analysis. However, a more sensitive method is desired that finds reliable results, even when the SEP is difficult to identify.

Potential biomarkers derived from source localization and source interactions

Additional processing steps such as source localization could further improve LI estimation. The LI is currently calculated from electrodes located above the sensorimotor cortex. However, electrodes above the sensorimotor cortex measure electric potential from more sources than just the sensorimotor cortex (Kakigi, 1986). This creates a possible source of error in calculating the LI from electrode data, as not all measured potentials originate in the sensorimotor cortex. Measured potentials that originate in the opposite hemisphere are especially problematic for accurate LI calculation. Source localization, where the spatial location of active sources is identified from its contribution to scalp electrodes (Jatoi et al., 2014), is a proposed solution to this problem. After source localization, estimated source activity in the sensorimotor cortex should not contain activity from neighboring sources. The LI estimated from source activity should be more sensitive than an LI derived from EEG channel data because non-related activity has been removed as noise.

A further step in processing would derive potential biomarkers from causal interactions between sources using VBMEG. Metrics derived from EEG data such as the LI or peak amplitude can quantify hemispheric differences but provide little insight into information flow between cortical sources. Other methods using EEG or MEG to investigate source dynamics included methods based purely on signal analysis, such as network analysis using graph theory (Smit et al., 2008; Stam et al., 2009), coherence (Srinivasan et al., 2007), or signal driven MAR modeling (Blinowska et al., 2004; Bressler & Seth, 2011). The VBMEG derived MAR model is constrained by anatomical information, decreasing false-positive connections (O. G. Filatova et al., 2018). The model computation constrained by anatomical connections further separates relevant brain activity from irrelevant brain activity compared to data obtained from source localization. For this reason, We expect that asymmetry metrics derived from VBMEG to be more sensitive than metrics derived from source localization and EEG channel data.

In order to compare LI results from the current research to results obtained from VBMEG, the LI should be calculated from the VBMEG data. Earlier research (Runfeng, 2018) proposed calculating the LI using the estimated MAR model:

$$LI = \frac{D_{contra} - D_{ipsi}}{D_{contra} + D_{ipsi}} \tag{5}$$

Where D is the number of parcels whose outward information flow strength is above the median z-score. The information flow strength is defined as the source activity

times the sum of absolute AR coefficients starting from this parcel. D_{contra} contains all parcels in the hemisphere contralateral to the stimulated limb, D_{ipsi} contains all parcels ipsilateral to the stimulated limb.

We propose a different strategy to calculate the LI of the VBMEG method. All top half parcels are treated equally by calculating the LI from the number of parcels with above-median z-score. The underlying information flow strength is not considered by assigning a D value from the number of parcels, which might skew results. This method performs poorly when both hemispheres have an equal amount of parcels with an above-median z-score, but the information flow of one hemisphere is significantly higher. Such a situation would have an LI of around zero, while the underlying difference in information flow is unequal. Another example is when all activity is located in a few parcels. In this situation, all included parcels will have equal weight in the LI. The D-values do not represent the underlying information flow strength. For these situations, the LI calculated as described in equation 5 does not reflect the underlying situation and is a potential source of error in future research.

A better approach would utilize the average information flow strength of parcels above the sensorimotor cortex. Such a metric is more similar to the LI from Vlaar et al. (Vlaar et al., 2017). This proposed improvement is in line with suggested improvements to fMRI derived LI's (Seghier, 2008). Only parcels in the region of interest would be incorporated instead of all parcels in a hemisphere. The D-value reflects the underlying information flow strength without discarding parcels. The LI remains bounded between -1 and 1.

Besides the LI, several other metrics can be computed to determine contralesional recruitment following a stroke. For example, the inter-hemispheric cross talk can be determined from the VBMEG model. The inter-hemispheric cross-talk is the number of nonzero parameters in the MAR model indicating interhemispheric connections. Earlier research (O. G. Filatova et al., 2018) found that inter-hemispheric connections in stroke subjects were more abundant than in healthy controls, indicating increased recruitment of the non-infarcted hemisphere. However, these metrics only quantify the level of lateralization. Ideally, we would identify active areas and processes during the recruitment of the non-infarcted hemisphere in addition to quantifying lateralization. The brain dynamics movie from the VBMEG toolbox allows for visualization of such a process, and the MAR coefficients can indicate quantitatively which areas are active and when. Other metrics could be computed in the frequency domain. Future analysis in the frequency domain is of interest, with a multisine input, the brain symmetry index could be calculated from the signal power. Many metrics can be derived from VBMEG, which could lead to new insight into functional changes during stroke recovery.

Limitations

There are several limitations to this work, and it could be improved in the following directions:

- The current research has a sample size of 5 patients. This is the dataset eligible for VBMEG analysis (dMRI and T1 MRI images obtained). In order to make broader claims about stroke, or clinically relevant conclusions, a larger sample size of longitudinal stroke subjects should be acquired. Making the data acquisition protocol for stroke patients less cumbersome could aid in recruiting a larger sample size. Currently, subjects are recruited upon admission to the hospital and subject to 4 EEG and (d)MRI measurements and clinical tests. The only remaining subjects have a good prognosis of recovery, while significantly affected subjects drop out. Future research should emphasize minimal patient burden to find a dataset with a larger sample size that is more representative of stroke subjects.
- No healthy controls are included in this study. Currently, the LI of a SEP is unknown for healthy individuals. Whether the observed trends in the LI are a return to healthy values is unknown. Future research should incorporate measurements of healthy controls.
- The LI is modeled to predict the FMA-UE using a linear mixed model. Future research could explore different model structures such as an exponential model to fit the data. These might reflect the data structure at higher FMA-UE values more adequate than a linear model and have shown new insight in previous studies (Van der Vliet et al., 2020). Future research could explore different models to explain the data distribution.
- All of the subjects in the dataset of five longitudinal stroke subjects are male. Literature has indicated differences in stroke incidence, treatment, and outcome between sexes(Appelros et al., 2010; Haast et al., 2012). Future research should include subjects of both sexes.
- The present study has not compensated for the applied stimulation amplitude in the SEP response. Previous research indicated that the SEP response is dependent on the stimulation amplitude (Arthurs et al., 2004; Backes et al., 2000). Patients were stimulated with an average of 5 ± 1.26 mA. It is difficult to determine how much this affects our results, as the effect likely varies strongly between healthy subjects and stroke patients, as well as between stroke patients.

Conclusions

The current study explored the possibility of quantifying potential biomarkers derived from EEG data along with the VBMEG method.

SEP peak amplitude and the LI were explored as potential biomarkers. SEP peak amplitudes were too inconsistent in identification, and the variation in amplitude was too large to be considered feasible as a biomarker using a dataset of this sample size.

Healthy controls and larger sample size are required to make clinically relevant conclusions on predicting stroke recovery using a biomarker. Nevertheless, we were able to demonstrate that metrics derived from asymmetry, such as the LI, have potential as a biomarker. Based on the trends in our dataset, the LI of the infarcted hemisphere shows potential as a biomarker for stroke recovery at low baseline FMA-UE.

In addition, the significant effect between the LI of the non-infarcted hemisphere and the FMA-UE is a surprising finding. While it might be attributed to remaining background cortical activity, it could also challenge current views on the laterality of SEP's and stroke recovery.

We were unable to recreate the discovered trend using an additional dataset of 17 longitudinal patients due to differences in pre-processing. The dataset should be pre-processed again with ICA included to perform our analysis reliably.

The goal of this research was to quantify asymmetry metrics from SEP's and determine their value as a biomarker for stroke recovery. We were able to quantify metrics from EEG channel data and investigate their value as a biomarker. However, we were unable to derive asymmetry metrics derived from dynamical source interactions using VBMEG.

In the future, we plan to quantify asymmetry metrics using source localization and VBMEG. Further separation of relevant brain activity from irrelevant brain activity is expected to lead to more sensitive metrics, novel quantifications of brain activity and pave the way for more effective neurorehabilitation approaches.

Bibliography

Allison, T., McCarthy, G., Wood, C. C., Darcey, T. M., Spencer, D. D., & Williamson, P. D. (1989). Human cortical potentials evoked by stimulation of the median nerve. II. Cytoarchitectonic areas generating short-latency activity. *Journal of Neurophysiology*, *62*(3), 694–710.

Al-Rawi, M. A. W., Hamdan, F. B., & Abdul-Muttalib, A. K. (2009). Somatosensory evoked potentials as a predictor for functional recovery of the upper limb in patients with stroke. *Journal of Stroke and Cerebrovascular Diseases*, *18*(4), 262–268.

Andersson, J. L. R., & Sotiropoulos, S. N. (2016). An integrated approach to correction for off-resonance effects and subject movement in diffusion MR imaging. *Neuroimage*, *125*, 1063–1078.

Appelros, P., Stegmayr, B., & Terént, A. (2010). A review on sex differences in stroke treatment and outcome. *Acta Neurologica Scandinavica*, *121*(6), 359–369.

Arthurs, O. J., & Boniface, S. J. (2003). What aspect of the fMRI BOLD signal best reflects the underlying electrophysiology in human somatosensory cortex? *Clinical Neurophysiology*, *114*(7), 1203–1209.

Arthurs, O. J., Johansen-Berg, H., Matthews, P. M., & Boniface, S. J. (2004). Attention differentially modulates the coupling of fMRI BOLD and evoked potential signal amplitudes in the human somatosensory cortex. *Experimental Brain Research*, *157*(3), 269–274.

Ashburner, J., & Friston, K. (1998). MRI sensitivity correction and tissue classification. *NeuroImage*, *7*(4), S706.

ATR Neural Information Analysis Laboratories. (2017, December 1). *User manual for DMRI data processing* .

ATR Neural Information Analysis Labs. (n.d.-a). *Connectome dynamics movie*. Retrieved July 20, 2021, from https://vbmeg.atr.jp/docs/v22/static/vbmeg2_dynamics_movie_creation.html

ATR Neural Information Analysis Labs. (n.d.-b). *Linear Connectome Dynamics estimation : Two-step method*. Retrieved July 20, 2021, from ATR Neural Information Analysis Labs., Kyoto, Japan

ATR Neural Information Analysis Labs. (2018, April 11). *VBMEG users manual*. https://vbmeg.atr.jp/docs/v22/static/vbmeg_users_manual.html#toc7

Backes, W. H., Mess, W. H., van Kranen-Mastenbroek, V., & Reulen, J. P. H. (2000). Somatosensory cortex responses to median nerve stimulation: fMRI effects of current amplitude and selective attention. *Clinical Neurophysiology*, *111*(10), 1738–1744.

Bajaj, S., Butler, A. J., Drake, D., & Dhamala, M. (2015). Brain effective connectivity during motor-imagery and execution following stroke and rehabilitation. *NeuroImage: Clinical*, *8*, 572–582.

Bastos, A. M., & Schoffelen, J.-M. (2016). A tutorial review of functional connectivity analysis methods and their interpretational pitfalls. *Frontiers in Systems Neuroscience*, *9*, 175.

Blinowska, K. J., Kuś, R., & Kamiński, M. (2004). Granger causality and information flow in multivariate processes. *Physical Review E*, *70*(5), 050902.

Boyd, L. A., Hayward, K. S., Ward, N. S., Stinear, C. M., Rosso, C., Fisher, R. J., Carter, A. R., Leff, A. P., Copland, D. A., & Carey, L. M. (2017). Biomarkers of stroke recovery: consensus-based core recommendations from the stroke recovery and rehabilitation roundtable. *International Journal of Stroke*, *12*(5), 480–493.

Bressler, S. L., & Seth, A. K. (2011). Wiener–Granger causality: a well established methodology. *Neuroimage*, *58*(2), 323–329.

Buma, F. E., Lindeman, E., Ramsey, N. F., & Kwakkel, G. (2010). Functional neuroimaging studies of early upper limb recovery after stroke: a systematic review of the literature. *Neurorehabilitation and Neural Repair*, *24*(7), 589–608.

Dale, A., Fischl, B., & Sereno, M. I. (1999). Cortical Surface-Based Analysis: I. Segmentation and Surface Reconstruction. *NeuroImage*, *9*(2), 179–194.

Delorme, A., & Makeig, S. (2004). EEGLAB: an open source toolbox for analysis of single-trial EEG dynamics including independent component analysis. *Journal of Neuroscience Methods*, *134*(1), 9–21. https://doi.org/10.1016/j.jneumeth.2003.10.009

Desmedt, J. E., & Cheron, G. (1980). Somatosensory evoked potentials to finger stimulation in healthy octogenarians and in young adults: Wave forms, scalp topography and transit times of parietal and frontal components. *Electroencephalography and Clinical Neurophysiology*, *50*(5–6), 404–425.

Druschky, K., Kaltenhäuser, M., Hummel, C., Druschky, A., Huk, W., Neundörfer, B., & Stefan, H. (2003). Somatosensory evoked magnetic fields following passive movement compared with tactile stimulation of the index finger. *Experimental Brain Research*, *148*(2), 186–195.

Dunning, K. (2011). Fugl-Meyer Assessment of Sensorimotor Impairment. In J. and C. B. Kreutzer Jeffrey S. and DeLuca (Ed.), *Encyclopedia of Clinical Neuropsychology* (pp. 1102–1103). Springer New York. https://doi.org/10.1007/978-0-387-79948-3_1806

Feigin, V. L., Mensah, G. A., Norrving, B., Murray, C. J. L., & Roth, G. A. (2015). Atlas of the global burden of stroke (1990-2013): the GBD 2013 study. *Neuroepidemiology*, *45*(3), 230–236.

Feigin, V. L., Nichols, E., Alam, T., Bannick, M. S., Beghi, E., Blake, N., Culpepper, W. J., Dorsey, E. R., Elbaz, A., Ellenbogen, R. G., & others. (2019). Global, regional, and national burden of neurological disorders, 1990–2016: a systematic analysis for the Global Burden of Disease Study 2016. *The Lancet Neurology*, *18*(5), 459–480.

Feys, H., van Hees, J., Bruyninckx, F., Mercelis, R., & de Weerdt, W. (2000). Value of somatosensory and motor evoked potentials in predicting arm recovery after a stroke. *Journal of Neurology, Neurosurgery & Psychiatry*, *68*(3), 323–331.

Fieldtrip. (n.d.). *How are the different head and MRI coordinate systems defined?* Retrieved July 19, 2021, from https://www.fieldtriptoolbox.org/faq/how_are_the_different_head_and_mri_coordinate_systems_defined/#how-are-the-different-head-and-mri-coordinate-systems-defined

Filatova, L. (2019). *A longitudinal diffusion MRI study: case studies from acute to chronic stroke*. https://doi.org/10.4233/uuid:38dffcc5-11fb-45c1-8de9-1d9fba72a395

Filatova, O. G., Yang, Y., Dewald, J. P. A., Tian, R., Maceira-Elvira, P., Takeda, Y., Kwakkel, G., Yamashita, O., & van der Helm, F. C. T. (2018). Dynamic Information Flow Based on EEG and Diffusion MRI in Stroke: A Proof-of-Principle Study. *Frontiers in Neural Circuits*, *12*. https://doi.org/10.3389/fncir.2018.00079

Fischl, B., & Dale, A. M. (2000). Measuring the thickness of the human cerebral cortex from magnetic resonance images. *Proceedings of the National Academy of Sciences of the United States of America*, *97*(20), 11050–11055.

Fischl, B., Salat, D. ~H., Busa, E., Albert, M., Dieterich, M., Haselgrove, C., van der Kouwe, A., Killiany, R., Kennedy, D., Klaveness, S., Montillo, A., Makris, N., Rosen, B., & Dale, A. ~M. (2002). Whole brain segmentation: automated labeling of neuroanatomical structures in the human brain. *Neuron*, *33*, 341–355.

Fischl, B., Sereno, M. I., & Dale, A. (1999). Cortical Surface-Based Analysis: II: Inflation, Flattening, and a Surface-Based Coordinate System. *NeuroImage*, *9*(2), 195–207.

Fischl, B., Sereno, M. I., Tootell, R. B. H., & Dale, A. M. (1999). High-resolution intersubject averaging and a coordinate system for the cortical surface. *Human Brain Mapping*, *8*(4), 272–284. https://doi.org/10.1002/(SICI)1097-0193(1999)8:4<272::AID-HBM10>3.0.CO;2-4

Fischl, B., van der Kouwe, A., Destrieux, C., Halgren, E., Ségonne, F., Salat, D. H., Busa, E., Seidman, L. J., Goldstein, J., Kennedy, D., Caviness, V., Makris, N., Rosen, B., & Dale, A. M. (2004). Automatically Parcellating the Human Cerebral Cortex. *Cerebral Cortex*, *14*(1), 11–22. https://doi.org/10.1093/cercor/bhg087

Fukushima, M., Yamashita, O., Knösche, T. R., & Sato, M. aki. (2015). MEG source reconstruction based on identification of directed source interactions on whole-brain anatomical networks. *NeuroImage*, *105*, 408–427. https://doi.org/10.1016/j.neuroimage.2014.09.066

Ganzetti, M., Wenderoth, N., & Mantini, D. (2016). Quantitative evaluation of intensity inhomogeneity correction methods for structural MR brain images. *Neuroinformatics*, *14*(1), 5–21.

Glover, G. H. (2011). Overview of functional magnetic resonance imaging. *Neurosurgery Clinics*, *22*(2), 133–139.

Graham, M. S., Drobnjak, I., & Zhang, H. (2016). Realistic simulation of artefacts in diffusion MRI for validating post-processing correction techniques. *NeuroImage*, *125*, 1079–1094.

Haast, R. A. M., Gustafson, D. R., & Kiliaan, A. J. (2012). Sex differences in stroke. *Journal of Cerebral Blood Flow & Metabolism*, *32*(12), 2100–2107.

Huang, M., Davis, L. E., Aine, C., Weisend, M., Harrington, D., Christner, R., Stephen, J., Edgar, J. C., Herman, M., & Meyer, J. (2004). MEG response to median nerve stimulation correlates with recovery of sensory and motor function after stroke. *Clinical Neurophysiology*, *115*(4), 820–833.

Jatoi, M. A., Kamel, N., Malik, A. S., Faye, I., & Begum, T. (2014). A survey of methods used for source localization using EEG signals. *Biomedical Signal Processing and Control*, *11*, 42–52.

Johansen-Berg, H., Rushworth, M. F. S., Bogdanovic, M. D., Kischka, U., Wimalaratna, S., & Matthews, P. M. (2002). The role of ipsilateral premotor cortex in hand movement after stroke. *Proceedings of the National Academy of Sciences*, *99*(22), 14518–14523.

Julkunen, L., Tenovuo, O., Jääskeläinen, S. K., & Hämäläinen, H. (2005). Recovery of somatosensory deficits in acute stroke. *Acta Neurologica Scandinavica*, *111*(6), 366–372.

Jung, P., Baumgärtner, U., Bauermann, T., Magerl, W., Gawehn, J., Stoeter, P., & Treede, R.-D. (2003). Asymmetry in the human primary somatosensory cortex and handedness. *Neuroimage*, *19*(3), 913–923.

Kajihara, S., Ohtani, Y., Goda, N., Tanigawa, M., Ejima, Y., & Toyama, K. (2004). Wiener filter-magnetoencephalography of visual cortical activity. *Brain Topography*, *17*(1), 13–25.

Kakigi, R. (1986). Ipsilateral and contralateral SEP components following median nerve stimulation: effects of interfering stimuli applied to the contralateral hand. *Electroencephalography and Clinical Neurophysiology*, *64*(3), 246–259.

Kalogianni, K., Daffertshofer, A., van der Helm, F. C. T., Schouten, A. C., & de Munck, J. C. (2018). Disentangling somatosensory evoked potentials of the fingers: limitations and clinical potential. *Brain Topography*, *31*(3), 498–512.

Kalogianni, K., de Munck, J. C., Nolte, G., Vardy, A. N., van der Helm, F. C. T., & Daffertshofer, A. (2018). Spatial resolution for EEG source reconstruction—A simulation study on SEPs. *Journal of Neuroscience Methods*, *301*, 9–17.

Kalogianni, K., Saes, M., Vlaar, M., van Wegen, E., Kwakkel, G., Schouten, A., van der Helm, F. C. T. , Daffertshofer, A., & de Munck, J. C. (2018). Are longitudinal SEP recordings a biomarker for proportional motor recovery post stroke? *Unpublished*. https://doi.org/doi.org/10.4233/uuid:2dceae5b-145f-41fd-9b08-200d1e4781af

Keren, O., Ring, H., Solzi, P., Pratt, H., & Groswasser, Z. (1993). Upper limb somatosensory evoked potentials as a predictor of rehabilitation progress in dominant hemisphere stroke patients. *Stroke*, *24*(12), 1789–1793.

Kim, S.-G., & Fukuda, M. (2008). Lessons from fMRI about mapping cortical columns. *The Neuroscientist*, *14*(3), 287–299.

Laaksonen, K., Kirveskari, E., Mäkelä, J. P., Kaste, M., Mustanoja, S., Nummenmaa, L., Tatlisumak, T., & Forss, N. (2012). Effect of afferent input on motor cortex excitability during stroke recovery. *Clinical Neurophysiology*, *123*(12), 2429–2436.

Lin, D. J., Cloutier, A. M., Erler, K. S., Cassidy, J. M., Snider, S. B., Ranford, J., Parlman, K., Giatsidis, F., Burke, J. F., Schwamm, L. H., & others. (2019). Corticospinal tract injury estimated from acute stroke imaging predicts upper extremity motor recovery after stroke. *Stroke*, *50*(12), 3569–3577.

Oliveira-Filho, J., & WJ, K. (2010). Initial assessment and management of acute stroke. *UpToDate. Waltham, MA: UpToDate. Retrieved January*.

Oostenveld, R., Fries, P., Maris, E., & Schoffelen, J.-M. (2011). FieldTrip: open source software for advanced analysis of MEG, EEG, and invasive electrophysiological data. *Computational Intelligence and Neuroscience*, *2011*.

Owen, M., Ingo, C., & Dewald, J. (2017). Upper extremity motor impairments and microstructural changes in bulbospinal pathways in chronic hemiparetic stroke. *Frontiers in Neurology*, *8*, 257.

Penny, W. D., Friston, K. J., Ashburner, J. T., Kiebel, S. J., & Nichols, T. E. (2011). *Statistical parametric mapping: the analysis of functional brain images*. Elsevier.

Prabhakaran, S., Zarahn, E., Riley, C., Speizer, A., Chong, J. Y., Lazar, R. M., Marshall, R. S., & Krakauer, J. W. (2008). Inter-individual variability in the capacity for motor recovery after ischemic stroke. *Neurorehabilitation and Neural Repair*, *22*(1), 64–71.

Pujol, J., Deus, J., Losilla, J. M., & Capdevila, A. (1999). Cerebral lateralization of language in normal left-handed people studied by functional MRI. *Neurology*, *52*(5), 1038.

Runfeng, T. (2018). *Brain Dynamic Information Flow Estimation Based on EEG and Diffusion MRI*.

Saes, M., Meskers, C. G. M., Daffertshofer, A., van Wegen, E. E. H., Kwakkel, G., & others. (2021). Are early measured resting-state EEG parameters predictive for upper limb motor impairment six months poststroke? *Clinical Neurophysiology*, *132*(1), 56–62.

Sato, M. A., Yoshioka, T., Kajihara, S., Toyama, K., Goda, N., Doya, K., & Kawato, M. (2004). Hierarchical Bayesian estimation for MEG inverse problem. *NeuroImage*, *23*(3), 806–826. https://doi.org/10.1016/j.neuroimage.2004.06.037

Schubert, R., Ritter, P., Wüstenberg, T., Preuschhof, C., Curio, G., Sommer, W., & Villringer, A. (2008). Spatial attention related SEP amplitude modulations covary with BOLD signal in S1—a simultaneous EEG—fMRI study. *Cerebral Cortex*, *18*(11), 2686–2700.

Seghier, M. L. (2008). Laterality index in functional MRI: methodological issues. *Magnetic Resonance Imaging*, *26*(5), 594–601.

Shelton, F. D. N. A. P., & Reding, M. J. (2001). Effect of lesion location on upper limb motor recovery after stroke. *Stroke*, *32*(1), 107–112.

Smit, D. J. A., Stam, C. J., Posthuma, D., Boomsma, D. I., & de Geus, E. J. C. (2008). Heritability of “small-world” networks in the brain: A graph theoretical

analysis of resting-state EEG functional connectivity. *Human Brain Mapping*, *29*(12), 1368–1378.

Smith, S. M., Jenkinson, M., Woolrich, M. W., Beckmann, C. F., Behrens, T. E. J., Johansen-Berg, H., Bannister, P. R., de Luca, M., Drobnjak, I., Flitney, D. E., Niazy, R. K., Saunders, J., Vickers, J., Zhang, Y., de Stefano, N., Brady, J. M., & Matthews, P. M. (2004). Advances in functional and structural MR image analysis and implementation as FSL. *NeuroImage*, *23*. https://doi.org/10.1016/j.neuroimage.2004.07.051

Soulard, J., Huber, C., Baillieul, S., Thuriot, A., Renard, F., Broche, B. A., Krainik, A., Vuillerme, N., & Jaillard, A. (2020). Motor tract integrity predicts walking recovery: a diffusion MRI study in subacute stroke. *Neurology*, *94*(6), e583–e593.

Spiegel, J., Tintera, J., Gawehn, J., Stoeter, P., & Treede, R.-D. (1999). Functional MRI of human primary somatosensory and motor cortex during median nerve stimulation. *Clinical Neurophysiology*, *110*(1), 47–52.

Srinivasan, R., Winter, W. R., Ding, J., & Nunez, P. L. (2007). EEG and MEG coherence: measures of functional connectivity at distinct spatial scales of neocortical dynamics. *Journal of Neuroscience Methods*, *166*(1), 41–52.

Stam, C. J., de Haan, W., Daffertshofer, A., Jones, B. F., Manshanden, I., van Cappellen van Walsum, A.-M., Montez, T., Verbunt, J. P. A., de Munck, J. C., & van Dijk, B. W. (2009). Graph theoretical analysis of magnetoencephalographic functional connectivity in Alzheimer's disease. *Brain*, *132*(1), 213–224.

Stolk-Hornsveld, F., Crow, J. L., Hendriks, E. P., van der Baan, R., & Harmeling-van Der Wel, B. C. (2006). The Erasmus MC modifications to the (revised) Nottingham Sensory Assessment: a reliable somatosensory assessment measure for patients with intracranial disorders. *Clinical Rehabilitation*, *20*(2), 160–172.

Suetens, P. (2009). *Fundamentals of Medical Imaging* (second edition). Cambridge.

Takeda, Y., Suzuki, K., Kawato, M., & Yamashita, O. (2019). MEG Source Imaging and Group Analysis Using VBMEG. *Frontiers in Neuroscience*, *13*. https://doi.org/10.3389/fnins.2019.00241

Tournier, J.-D., Calamante, F., Gadian, D. G., & Connelly, A. (2004). Direct estimation of the fiber orientation density function from diffusion-weighted MRI data using spherical deconvolution. *Neuroimage*, *23*(3), 1176–1185.

van der Vliet, R., Selles, R. W., Andrinopoulou, E., Nijland, R., Ribbers, G. M., Frens, M. A., Meskers, C., & Kwakkel, G. (2020). Predicting upper limb motor

impairment recovery after stroke: a mixture model. *Annals of Neurology*, *87*(3), 383–393.

Vatta, F., Bruno, P., & Inchingolo, P. (2000). Accuracy of EEG dipole source localisation in presence of brain lesions. *Biomedical Sciences Instrumentation*, *36*, 403–408.

Vatta, F., Bruno, P., & Inchingolo, P. (2002). Accuracy of EEG source reconstruction in the presence of brain lesions: modelling errors and surface electrodes' placement. *Biomedical Sciences Instrumentation*, *38*, 423–428.

Vatta, F., Bruno, P., & Inchingolo, P. (2001). EEG source localization sensitivity due to brain lesions modeling errors. *2001 Conference Proceedings of the 23rd Annual International Conference of the IEEE Engineering in Medicine and Biology Society*, *1*, 913–916.

Vlaar, M. P., Solis-Escalante, T., Dewald, J. P. A., van Wegen, E. E. H., Schouten, A. C., Kwakkel, G., & van der Helm, F. C. T. (2017). Quantification of task-dependent cortical activation evoked by robotic continuous wrist joint manipulation in chronic hemiparetic stroke. *Journal of Neuroengineering and Rehabilitation*, *14*(1), 1–15.

Winters, C., van Wegen, E. E. H., Daffertshofer, A., & Kwakkel, G. (2015). Generalizability of the proportional recovery model for the upper extremity after an ischemic stroke. *Neurorehabilitation and Neural Repair*, *29*(7), 614–622.

Yamada, H., Abe, O., Shizukuishi, T., Kikuta, J., Shinozaki, T., Dezawa, K., Nagano, A., Matsuda, M., Haradome, H., & Imamura, Y. (2014). Efficacy of distortion correction on diffusion imaging: comparison of FSL eddy and eddy_correct using 30 and 60 directions diffusion encoding. *PloS One*, *9*(11), e112411.

Yeh, F.-C., Tang, P.-F., & Tseng, W.-Y. I. (2013). Diffusion MRI connectometry automatically reveals affected fiber pathways in individuals with chronic stroke. *NeuroImage: Clinical*, *2*, 912–921.

Appendix A: Flowchart

Variational Bayesian Multimodal EncephaloGraphy

The VBMEG tutorial script was modified to our own needs. VBMEG can be opened using a GUI to enter commands and parameters. In our opinion, a script to recruit the required functions and parameters is more transparent and allows for easy reproduction of results and data transfer.

The script is set up in the following way:

The create_project function creates the required output directories, names, and paths for almost all scripts. In addition, this function contains parameters for various functions used later on in the VBMEG toolbox. The create_project function was altered to contain all parameters relevant for the processing pipeline. This function also sets the host and number of threads that will be used for fiber tracking. More information on setting up the host or localhost can be found in appendix B or the dMRI user manual (ATR Neural Information Analysis Laboratories, 2017)

The VBMEG toolbox uses its functions within Matlab or uses Matlab to create a system command to recruit an external program, which it then executes from Matlab. For example, when using Freesurfer to create a cortical model, the VBMEG toolbox creates a command line with the required inputs to run Freesurfer from a terminal and then runs this command using the system() function from Matlab.

Figure 9 displays the complete flowchart of the VBMEG pipeline. Blue boxes indicate inputs, yellow boxes indicate processing steps, and green boxes indicate outputs.

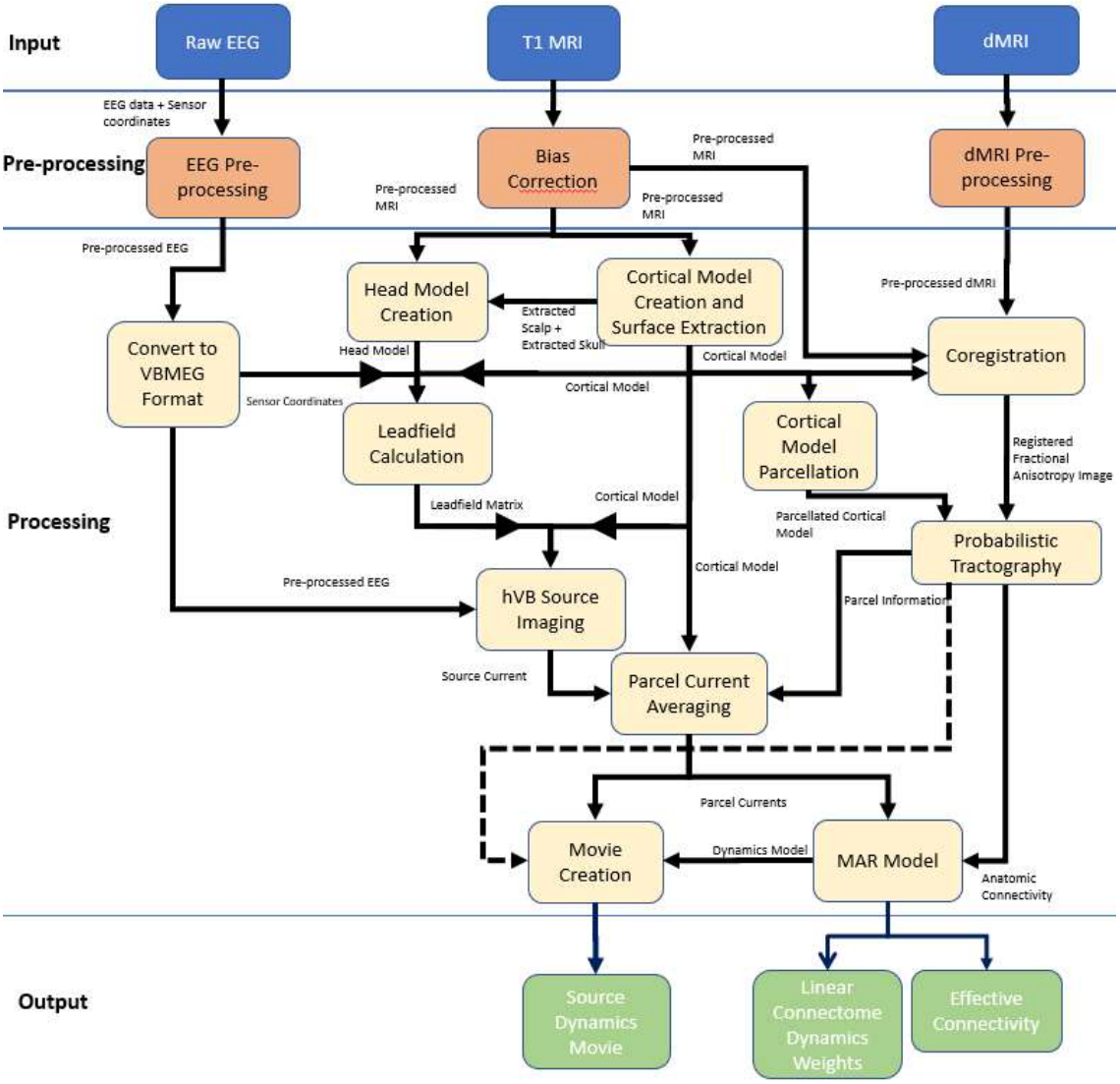

Figure 9 Flowchart of main VBMEG pipeline. Input blocks are displayed as blue, pre-processing blocks as orange, processing blocks as yellow and output blocks as green.

EEG Pre-processing

For pre-processing of EEG data, see the EEG Pre-Processing section of chapter 2.

MRI Bias Correction

Input: T1 MRI image (.nii)

Output: Bias corrected T1 MRI (.nii)

MRI Bias is a low-frequency smooth signal that corrupts MRI images (Ashburner & Friston, 1998; Ganzetti et al., 2016). The bias field decreases the performance of image processing algorithms that use gray level values, e.g., texture analysis or segmentation algorithms. The goal of bias correction is to ensure the overall conformity of intensity values for all tissues. VBMEG corrects for bias in MR images using SPM8 (Penny et al., 2011).

Image Segmentation

Input: Bias corrected T1 MRI image

Output: SPM normalization file, T1 MRI segmentation file (gray matter)

Image segmentation is an optional step during VBMEG. The VBMEG image segmentation function has two outputs: an SPM normalization file and a T1 MRI segmentation file.

The SPM normalization file is used to unnormalize fMRI activities analyzed on a standard brain towards an individual brain. As our data does not use fMRI, this file is redundant.

The segment function can be used to extract a gray matter image from the subject's brain. The resulting gray matter image can be used as a mask during head model creation. The gray matter image ensures that the head model does not intrude into the cortex. As such, this is an optional step to improve performance.

Before segmentation, a bias correction is also applied as this is built-in into SPM8 image segmentation. The bias correction step does not make the previous bias correction step redundant as later steps in the VBMEG pipeline do not use the outputs from this processing step.

Cortical Model Creation and Surface Extraction

Input: T1 MRI image

Output: Freesurfer Cortical model files, extracted scalp, extracted skull

The subsequent processing step creates the cortical model used to create the leadfield matrix and the head model. Freesurfer (Dale et al., 1999; Fischl et al., 2002, 2004; Fischl, Sereno, & Dale, 1999; Fischl, Sereno, Tootell, et al., 1999; Fischl & Dale, 2000) is used to create the head model. The steps of cortical model creation can be broken down into the following steps:

1. The function vb_freesurfer.m is called
2. VBMEG activates a c shell script called runfreesurfer.csh. This script aims to create all required output files and folders in the correct layout for VBMEG for subsequent processing steps.
3. The function vb_freesurfer.m runs the following command in the system (so not in Matlab). The script line is: recon-all -subject \$SUBJECTS_ID -i \$IMAGE_FILE -all.
   - recon-all performs all, or any part of, the FreeSurfer cortical reconstruction process
   - subject \$SUBJECTS_ID indicates the name of the subject used (is extracted from the Matlab parameters)
   -i \$IMAGE_FILE indicates the input file.
   - all indicates all steps must be performed, including cortical segmentation.

   It is possible to run Freesurfer from the command line outside VBMEG using the command line and Freesurfer commands. In this case, the user must make sure all required output files are saved in the correct folder for subsequent processing steps.

   Freesurfer creates a polygon model of the cortical surface. This polygon model is used in later processing steps for parcellation, head model creation, and leadfield calculation.

   More info on recon-all: https://surfer.nmr.mgh.harvard.edu/fswiki/recon-all

Head Model Creation

Input: cortical model, extracted scalp, extracted skull, T1 MRI image, gray matter image

Output: BEM head model

This step creates the head model used in the forward problem of source localization. A spherical model can be used as a head model for source localization, but a head model can be created from MRI data to obtain more accurate results. The VBMEG toolbox uses the function vb_job_head_3shell.m to create the head model.

The required files for this step are:

- A gray matter image obtain during the segmentation step
- Inner skull and outer skin surface files created during the creation of the cortical model
- The T1 MRI file (.nii format)
- The cortical model

A three-layer head model is created (CSF, Skull, Scalp) from the specified files. The model is created using the Boundary Element Method (BEM), implemented in the VBMEG toolbox (Takeda et al., 2019). If no individual model is available, a standard three-layer BEM head model can be used. When using patients with lesioned brains, care must be taken in this step to make sure the lesion does not affect source

localization, e.g., a lesion near the cortical surface or of large size. If the lesion is located in an area that would affect source localization, a correction must be applied to the head model to account for this lesion (Vatta et al., 2000)

Leadfield Calculation

Input: BEM head model, electrode locations, cortical model

Output: leadfield matrix

This is the forward problem step in source localization. The leadfield calculation is done by the function vb_job_leadfield.m. The leadfield matrix indicates how the activity of dipoles leads to electrode activity on the scalp. Calculation of the leadfield matrix in the VBMEG toolbox requires the following inputs:

- The head model (calculated in previous steps)
- The cortical model
- The electrode locations

An important step is to ensure the electrodes are in the same coordinate system as the MRI images. VBMEG's used coordinate system is named "SPM_right_m," according to the user manual (ATR Neural Information Analysis Labs, 2018). However, a literature search found no mention of the specific SPM_right_m coordinate system. Although it is probably a variant of the coordinate system used by SPM, SPM has traditionally used two coordinate systems over the last years. Older SPM versions use the Analyze coordinate system developed by the Mayo Clinic, and use LAS orientation (Fieldtrip, n.d.). A newer version of SPM uses the MNI coordinate system, which has RAS orientation with the center located at the anterior commissure (Fieldtrip, n.d.).

However, according to the latest VBMEG article (Takeda et al., 2019), the VBMEG coordinate system uses a RAS orientation with the origin at the center of the image in meters. This coordinate system seems to be a variant of the Freesurfer coordinate system with units in meters instead of mm. Coregistration of electrode coordinates to VBMEG coordinates is done by aligning the electrode location to skull landmarks. The Left and Right Pre-Auricular (LPA and RPA) points and the nasion fiducial point were measured during EEG acquisition by a 3D-pointer. These skull landmarks can be identified on an MRI image. The electrode locations can be registered to these points by a linear registration transforming the electrode locations to the correct coordinate system.

The leadfield matrix can be calculated from the head model, the cortical model, and the electrode locations. The conductivity settings for CSF, skull, and scalp can be set in this step, or standard values from the VBMEG toolbox can be used (Takeda et al., 2019).

hVB Source Imaging

Input: leadfield matrix, pre-processed EEG, cortical model

Output: source currents

The next step is the inverse problem in source localization, i.e., determining the dipoles from measured electrode signals. The inverse problem is ill-posed as the number of possible dipoles generally outnumbers the number of electrodes. As such, this is an equation with more unknowns than equations, and therefore, it does not have a unique solution.

The VBMEG toolbox uses its own source localization algorithm known as hierarchical Variational Bayesian source localization (Sato et al., 2004). The VBMEG Toolbox breaks the source imaging down into two steps: estimating the current variance and estimating the source current.

In the first step, estimating the current variance, the current variance is estimated from the EEG data. The current variance is estimated by the function vb_job_vb.m, and the required inputs are:

- The cortical model
- The leadfield matrix
- EEG data
- Optionally fMRI data can be added here, which we do not have

In addition, VBMEG requires several other parameters to be set to perform source localization. Such as time window, smoothness filter radius, noise model parameters, and more. Default values can be used, for more comprehensive information on these parameters and their meaning, see: https://vbmeg.atr.jp/docs/v22/static/vbmeg_users_manual.html#toc8

The next step is estimating the source current. This is performed by the function vb_job_current. The source current is estimated by calculating the inverse filters and calculating the current variance from the available data.

The function vb_job_current requires the following inputs

- The current variance obtained in the previous step.
- EEG data

The resulting file "*.curr.mat" contains the current timecourse information that will be used in further processing steps. The obtain source currents can also be viewed to determine if the source localization provided accurate results.

Connectome Dynamics Estimation

The next main chapter of the VBMEG Toolbox can be summarized as connectome dynamics estimation. The previous steps were encompassing source localization steps from EEG data combined with information from structural MRI. The following steps will encompass dMRI pre-processing, fiber tracking, and later, combing fiber tracking information with source localization to create a MAR model.

dMRI Pre-processing

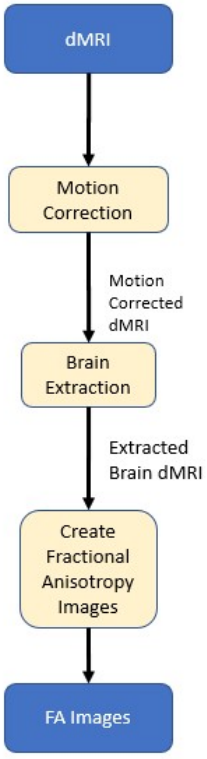

Figure 10: overview of dMRI pre-precessing. dMRI images are loaded and motion-corrected. The dMRI brain is extracted, and Fractional Anisotropy (FA) images are created.

Motion Correction

Input: dMRI image(s)

Output: motion corrected dMRI image(s)

The first step in dMRI processing is motion correction. Motion during dMRI recording can lead to a variety of artifacts in the dMRI image. The VBMEG toolbox has a motion correction function built-in using SPM. dMRI motion is corrected by the function dmri_4D_image_correct.m. The function calls to FSL from the VBMEG toolbox to use the motion correction using inputs specified from Matlab.

The implemented FSL function used for motion correction is FSL eddy_correct, an older version of the motion correction function currently employed by FSL. The new function is called eddy and has been shown to lead to improved motion correction results compared to its predecessor (Andersson & Sotiropoulos, 2016; Graham et al., 2016; Yamada et al., 2014) Eddy_correct is based on a classical affine transformation and uses a 12-dof affine transformation and correlation ratio as a cost-function to register the diffusion-weighted images to a b = 0 image (Yamada et al., 2014)

Pre-processed dMRI images are available in our case, as the available data has already been motion-corrected using FSL eddy_correct (L. Filatova, 2019). However, another motion correction step could be applied for improved results using the newer FSL eddy.

Brain Extraction

Input: motion-corrected dMRI image

Output: extracted dMRI brain image (dMRI brain)

In this section, the brain is extracted from the dMRI image. The brain is extracted using the -bet function by FSL. VBMEG uses the function brain_image_extract.m to extract the brain from the dMRI image. As with other functions, the main job for this function is to create the correct systems commands for FSL and run FSL with the desired inputs. In addition, a brain mask is created for later processing steps.

Create Fractional Anisotropy (FA) Image

Input: dMRI brain, brain mask image

Output: FA image

A Fractional Anisotropy (FA) image is created from the dMRI data. In the FA image, the principle diffusion direction is encoded by color and the degree of anisotropy by intensity. The FA image shows the anisotropic diffusion of water molecules in the brain's white matter fibers (Suetens, 2009)

The VBMEG toolbox creates an FA image using DTIFIT by FSL (Smith et al., 2004). (see: https://fsl.fmrib.ox.ac.uk/fsl/fslwiki/FDT/UserGuide#DTIFIT) . DTIFIT is an FSL function that fits a diffusion tensor model at each voxel and can create an FA image.

Coregistration

Input: cortical model, FA image, T1 MRI image

Output: transformation matrices in all directions (6 matrices)

In the coregistration block, we register the T1 MRI, Freesurfer cortical model FA image to the same space. A transformation matrix is made for every space to all other spaces allowing transfer from one image space to another. The shell script make_transwarp.sh performs Coregistration and is recruited through Matlab. Make_transwarp.sh is a VBMEG toolbox shell script that creates the nonlinear transformation matrices using FLIRT, FNIRT, and convertwarp from the FSL toolbox.

Transformations made:

- Freesurfer to T1 and back.
- T1 to diffusion and back.
- Freesurfer to diffusion and back.

Parcel Cortical Model

Input: cortical model, the desired number of parcels

Output: parcellated cortical model

In this section, the brain is parcellated into smaller regions. First, the cortical model is parcellated into parcels or ROI's using the function parcel_cortical_surface.

The number of parcels is a parameter that can be chosen by the user and ultimately determines the number of weights in the MAR model in the last step of the flowchart. The VBMEG toolbox standard number of parcels is 2000. Research on a similar dataset (O. G. Filatova et al., 2018) used 250 parcels to calculate the final model.

Important to note that the computation time increases quadratically with the number of parcels. In the case of 2000 parcels, a strong computer is required.

The parcellation of the cortical model seems to be as follows: first, the vertices used for the parcels are selected using the function dmri_vbmeg_vertex_select. X vertices are selected as parcels in this function, where X equals the number of selected parcels. The neighboring vertices in the cortical brain model are found from these X vertices by searching for near neighbors using vb_find_near_member. Vertices in the cortical model are distributed over all parcels using a maximum size parameter (default = 4 cm) and located near neighbors.

Authors note: The above explanation of parcellation suggests that parcellation is based on distance alone. One would expect the outcome to show somewhat circular-shaped parcels constrained by the cortical model. Figure 12 shows the parcellation of the left hemisphere. The shape of the parcellations is not as circular as initially expected, leading to the hypothesis of some further constraint applied during the neighbor search or vertex selection. Whether another constraint is present is currently unknown; a further investigation into the function can lead to more information. Otherwise, ATR can be approached for a further explanation. **End note**

The selected vertices are checked only to contain cortical vertices. Subcortical vertices are removed. Parcel.mat and membership.mat files are created as output. The parcel file contains the indices for all vertices for the left and right hemispheres and two different indices for each hemisphere. The membership.mat file contains information on the relation of parcel to brain model.

Probabilistic Tractography

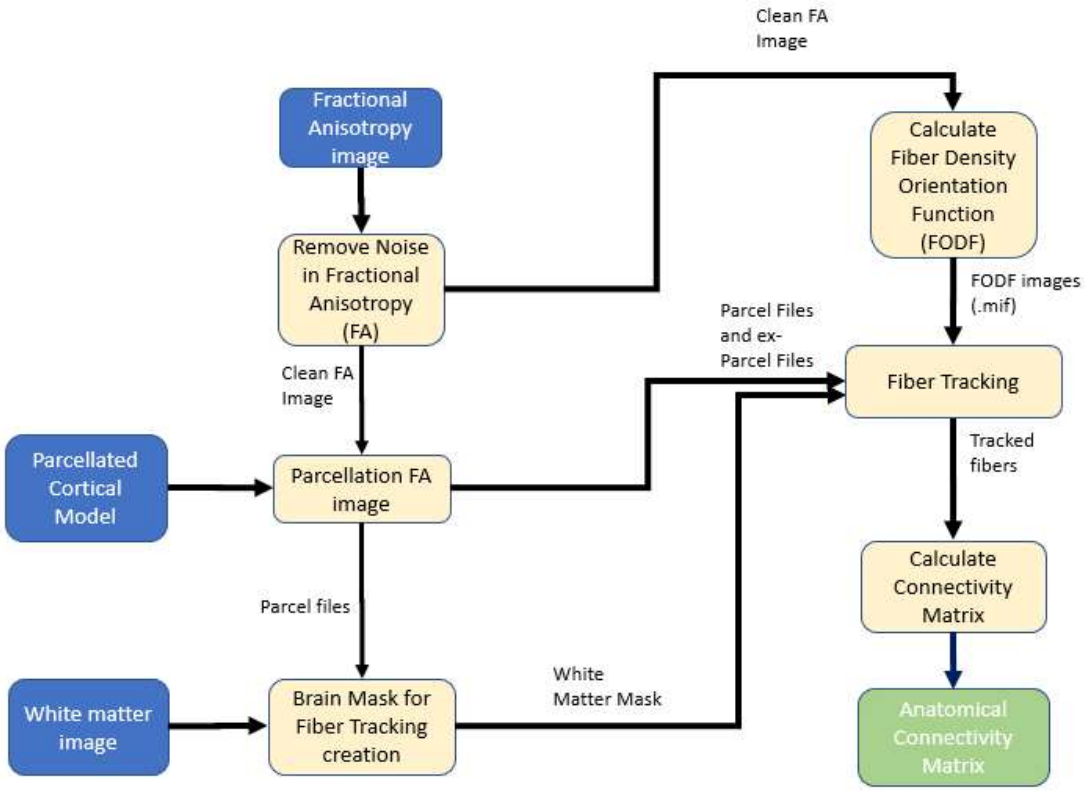

Figure 11: Probabilistic tractography flowchart. After noise removal, FA images are parcellated. A mask is created to support fiber tracking, and fiber tracking is performed using parcel information and the fiber orientation density function. An anatomical connectivity matrix is calculated from the fiber tracking output that is used during the estimation of the MAR model.

Remove Noise in Fractional Anisotropy Image

Input: FA image, brain mask

Output: corrected FA image

After previous processing steps, the FA image contains noise around the brain edges, presented as white dots. The MRI brain mask can be used to remove this noise. We use the Brain mask extracted from the T1 image to remove the noise and create a clean FA image.

The VBMEG toolbox transforms the extracted brain mask and MRI brain to FA space and then recreates the FA image as done in the earlier step. The newly created FA file should not contain any white noise dots around the edges. The function

remove_noise_in_fa.m removes the noise using dmri_image_transform and dmri_FA_image_create to recreate the FA image.

Parcellation FA Image

Input: parcellated cortical model, FA image

Output: parcel files, ex-parcel files

Important note: This step creates many temporary files that are removed at the end of the function. If the function is terminated early manually or due to an error, these files may not be removed. Multiple terminations of the script could lead to file cluttering and storage overflow. **End note.**

In this step, the vertices that are selected for parcels are converted into parcel files. The parcel files are binary .nii files that, when loaded, show a small part of the cortex.

Creating parcellated FA images is done in two steps. In the first step, all parcel information from the previous step is used to create X .label files, where X is the number of parcels. These .label files are in Freesurfer space and are in the correct format to be converted to volume files by FSL in later steps.

The next step is creating volumes from the label files. The function dmri_label_file_to_FA_volume creates FA volumes from the .label files.
First, Freesurfer (FS) volume files are created from the .label files using Freesurfer's mri_label2vol. The output volumes are transformed to struct files and FA volume files using FSL's FLIRT.

In addition, parcel-ex files are created. These files are the inclusion region of interest used in fiber tracking later. The parcel file is the seed region of interest, and the parcel-ex files the inclusion region of interest. The seed is the starting point for fiber tracking, the inclusion region of interest is the region where fibers are tracked from the seed point.

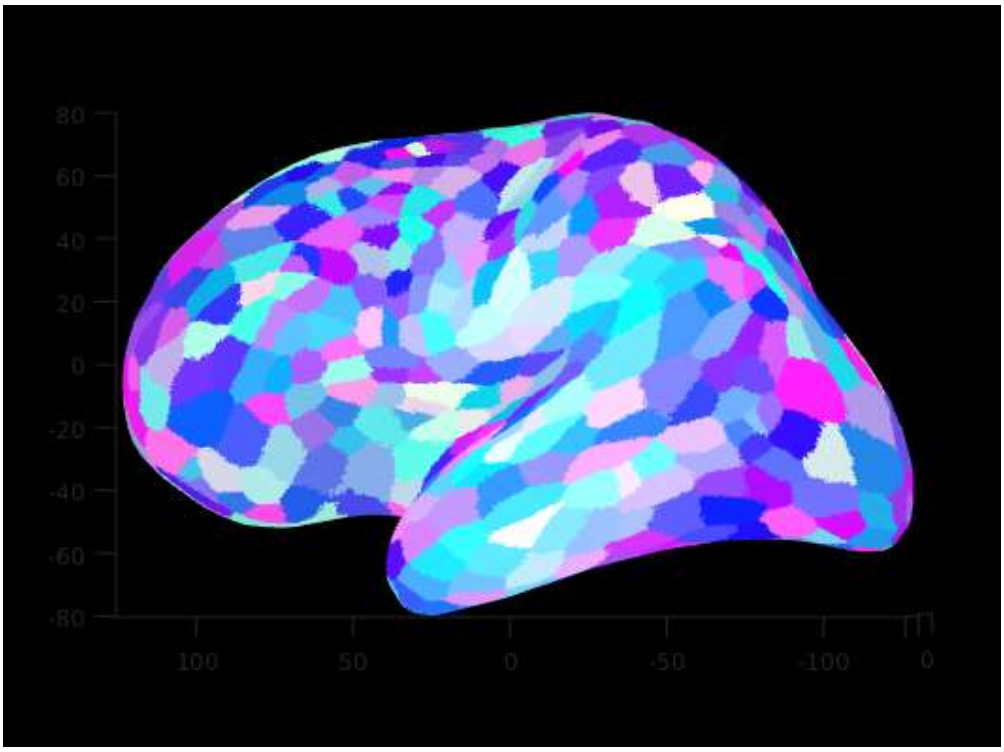

Figure 12: an overview of parcellation of the left hemisphere with 250 parcels (125 per hemisphere).

Create Mask for Fiber Tracking

Input: parcel files, white matter volume

Output: brain mask

A mask is created from the parcellated files. The mask is created by merging all parcel files with the white matter volume obtained in earlier processing steps. The mask supports fiber tracking to make sure no fibers are tracked that exit the brain volume.

From the parcellated files, we create a mask used in fiber tracking. The function create_mask_for_fiber_tracking from the VBMEG toolbox is used to create a mask. The function uses Freesurfer to create a white matter volume in FA space and FSL to merge the parcels and white matter to create a mask.

Calculate Fiber Orientation Density Function (FODF)

Input: FA image

Output: FODF information (.mif file)

Important note: This step uses MRTRix (http://jdtournier.github.io/mrtrix-0.2/index.html). The VBMEG toolbox is set up to perform all MRTRix functions on an external host. These processes can run on the localhost, but the correct sep-up is required. Information on setting up the external- or localhost can be found here: https://vbmeg.atr.jp/docs/v22/attachFile/vbmeg_users_manual/dmri_data_processing_en.pdf.
End note.

We calculate the Fiber Density Orientation Function (FODF) from the FA images used in fiber tracking. The FODF image contains ellipses containing the estimated orientation and density of fibers for all voxels in the brain. The fiber orientation density of some voxels is displayed in figure 13. The VBMEG toolbox uses the probabilistic fiber tracking algorithm from MRTRix, and this algorithm requires the fiber orientation density function as an input. If other methods of fiber tracking are desired, a different input may be required.

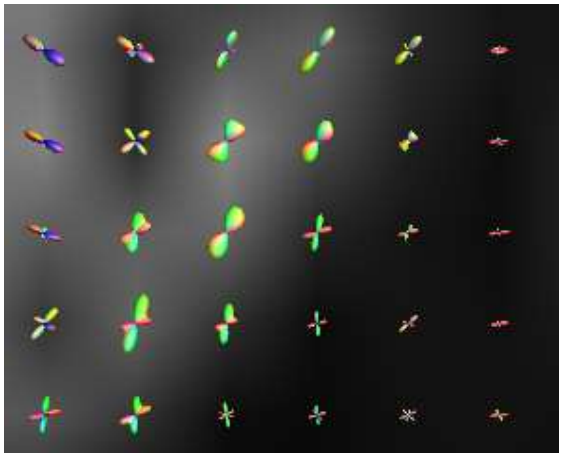

Figure 13 The fiber orientation density function of some voxels.The colors red, green, and blue indicate the direction of the major eigenvector of the diffusion tensor (Tournier et al., 2004). *The ellipses display the fiber orientation and density.*

The VBMEG toolbox calculates the FODF using the estimate_response and csdeconv functions from the MRTRix package. Estimate_response estimates the fiber response function, and csdeconv performs non-negativity constrained spherical deconvolution.

For more information on these functions, see:

https://jdtournier.github.io/mrtrix-0.2/commands/csdeconv.html

https://jdtournier.github.io/mrtrix-0.2/commands/estimate_response.html

Fiber Tracking

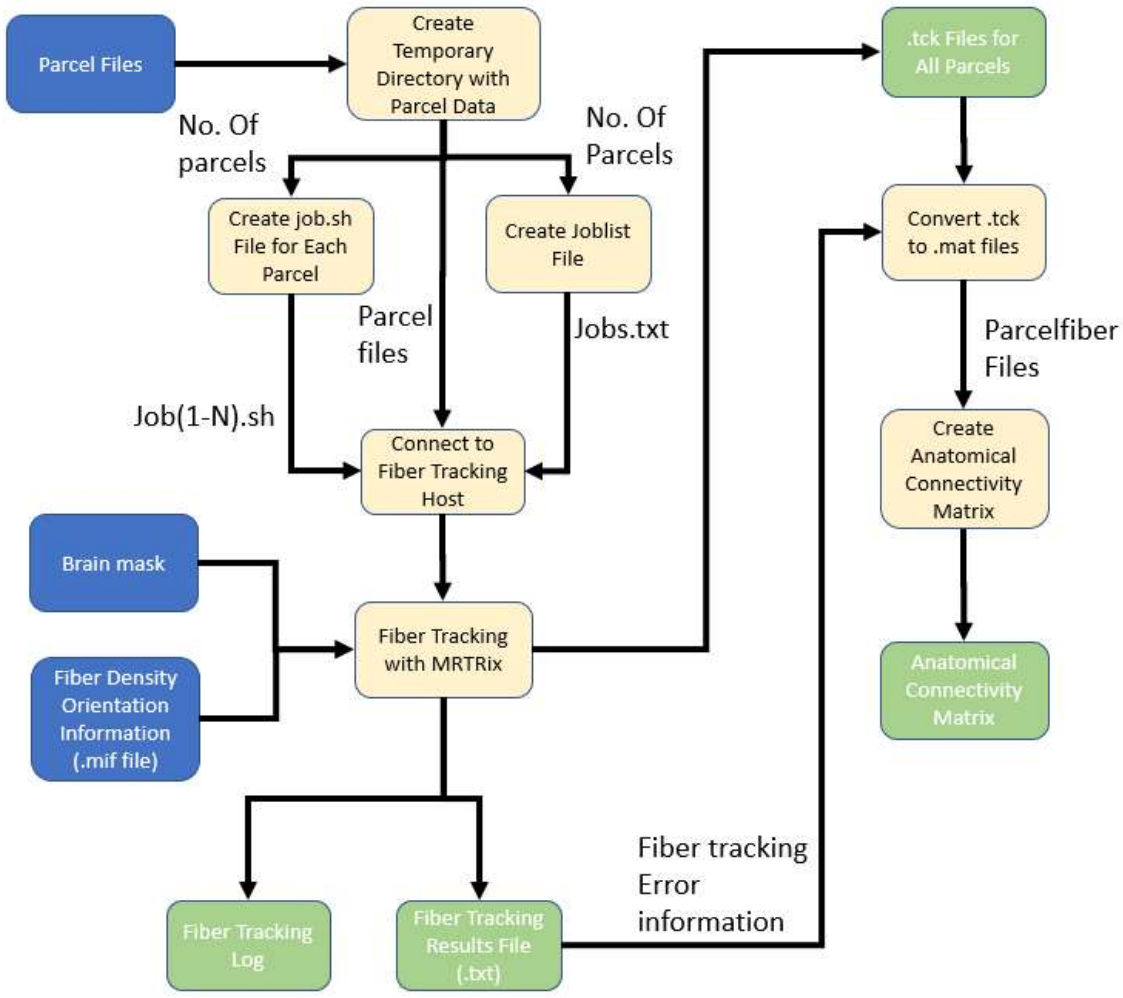

Figure 54 Flowchart of Fiber tracking. Parcel files, a brain mask, and the fiber orientation density function are used as inputs. Fibers are tracked from each parcel to each other parcel using an external host. This is the most computationally heavy step in the toolbox, and computation time increases quadratically with the number of parcels.

Input: parcel files, ex-parcel files, FODF information, brain mask

Output: parcel fiber files

Important note: This step uses MRTRix. The VBMEG toolbox is set up to perform all MRTRix functions on an external host. These processes can run on the localhost, but the correct sep-up is required. Information on setting up the external- or localhost can be found here:

https://vbmeg.atr.jp/docs/v22/attachFile/vbmeg_users_manual/dmri_data_processing_en.pdf **End note.**

Important note: This step creates many temporary files that are removed at the end of the function. If the function is terminated early manually or due to an error, these files may not be removed. Multiple terminations of the script could lead to file cluttering and storage overflow. **End note.**

Figure 14 shows the flowchart of fiber tracking as performed by the VBMEG toolbox. The function dmri_fiber_track_prob performs fiber Tracking. First, the VBMEG toolbox creates a temporary working directory with all required parcel data. From the data, several .txt files are created. The first .txt file is named Jobs.txt, and this file contains a list of jobs to be performed. This file is simply a list of locations for all fiber track.sh files that will be executed from this file.

In addition, for every parcel, a fiber_track(X).sh file is created. This file contains the required commands as a shell script to perform fiber tracking for Parcel X. This shell file contains the required commands for MRTRix to perform fiber tracking, streamtrack SD_PROB, which is MRTRix's version of probabilistic tractography. All jobs are divided over all "workers". Each worker is a single processor that can be utilized for fiber tracking. The number of threads can be set up in the function create_project in the beginning.

At this point, the actual fiber tracking is performed. Fiber tracking requires the FODF (.mif file) information from the previous step as input. The seed is the parcel for which fiber tracking is performed. Included regions in fiber tracking are all other parcels. A white matter mask is used to exclude connections outside the brain. In order to speed up the calculation, the maximum number of tracks to be generated can be decreased. However, this will lead to a coarser result.

Fiber tracking can be performed on the external host or the localhost. A log file, a results file, and X .tck files are created, one for each parcel. The results file contains information on whether an error occurred during fiber tracking for each parcel. The VBMEG toolbox then converts all .tck files into .mat files, which can be used for further processing. From the .mat files, a binary anatomical connectivity matrix is created. This file contains information on anatomical connections for each parcel to all other parcels. As such, the dimension of this matrix is parcel x parcel.

Important note: A bug seems to be present in this part of the VBMEG toolbox. The result.txt file contains a list of whether or a job was successful. When an error occurred, the toolbox should register the error and terminate the function. Unfortunately, this is not the case. When an error occurs, the toolbox continues and freezes later, during conversion to .mat files. Not all required .tck files are created, and the toolbox displays that it is still converting .tck files, while all available .tck files

are already converted. This issue was fixed by reading all results simultaneously, terminating if an error occurred, and was incorporated in the installation script. Due to the way the script is organized, we believe the design intention was to create a single result file for each parcel. This allows the erroneous parcel to be detected easily. A more elegant solution could integrate this solution into the VBMEG toolbox.

Unsolved issue: Currently, fiber tracking is not working perfectly. An error occurs in some cases of fiber tracking. In some cases, fiber tracking does not create a .tck file from parcel files. This is because input parcel.nii files are empty. Loading these files into a niftii viewer displays that the parcel has no volume. An error seems to occur during parcellation, where empty parcels are created. Further investigation showed that the error already occurs during parcellation of the cortical model, but it is unclear exactly where.

VBMEG's near neighbor algorithm found vertices with no near neighbors in the cortical model. Currently, the explanation behind creating empty parcels is speculation at best.
An error may occur during the near neighbor search, finding no neighbors for specific vertices. Perhaps the cortical model has some errors during creation, and the cortical model is not created correctly. Decreasing the number of parcels seems to solve the problem but decreases the resolution.

Ideally, empty parcels should not be a problem. The algorithm should detect empty parcels and exclude them from the analysis. The suggested solution would therefore include a check during parcellation and exclude empty parcels.

The text below displays the content of an empty .label file. Every line indicates a vertex in this .label file. Most files have ±200 vertices, and this file has one vertex indicating it has no volume. Information on the structure of a .label file can be found here: https://surfer.nmr.mgh.harvard.edu/fswiki/LabelsClutsAnnotationFiles.

#!ascii label, from subject /data/Gertrand_Thom/VBMEG_NEW/tutorial/program/../analyzed_data/s006/dmri/parcels/parcels.mat
1
132599 29.455973 37.216026 2.503677 0.000000

Calculate Connectivity Matrix

Input: parcel fiber files

Output: anatomical connectivity matrix, fiber length matrix

From fiber tracking results, we create the connectivity matrix displaying the connection between all parcels. The Connectivity matrix is a binary matrix containing information on the fiber connection of each parcel to all other parcels. The anatomical connection is binarized by a threshold connection strength (Default value: 1e-4), parcel connections lower than the threshold are deemed unconnected.

In addition, a fiber length matrix is calculated. First, time delays are calculated with the formula, from (ATR Neural Information Analysis Labs, n.d.-b):

$$\Delta t = \frac{f_l}{v} + \tau \tag{6}$$

Where Δt is the time delay, f_l is the fiber length, v (6 m/s) is the conduction velocity, and tau (27 ms) is the axonal time delay. The fiber length is obtained from fiber tracking output.

Matrices are created with time delays from every parcel to each other parcel and fiber lengths from each parcel to all other parcels. The function dmri_connect_parm_calc from the VBMEG toolbox calculates the connectivity matrix.

Parcel Current Averaging

Input: Source currents, parcel information

Output: parcel currents

In this section, the source current information is averaged over all parcels. The function calculate_roi_current from the VBMEG toolbox averages the source currents into each parcel.

MAR Model

Input: anatomical connectivity matrix, fiber length matrix, parcel currents

Output: MAR model

In this section, the MAR model is calculated. The model is estimated using estimate_dynamics_model and lcd_fitl2reg_holocalAR from the VBMEG toolbox. The MAR model is calculated using the anatomical connectivity matrix, fiber length matrix, and parcel currents from previous steps. Causal relations between parcel are inferred using

$$Z_{n,t} = \sum_{a=1}^{p} a_{nd} z_{n,t-d} + \sum_{v \epsilon C_n} b_{nv} z_{v,t-\Delta t_n} + \varepsilon_n \quad (7)$$

Where ***p*** is the order of self-influence, assumed to be 2. $z_{n,t}$ is the current density at time ***t*** of parcel n, $a_{n,d}$ is the local dynamics. C_n is an index set of structurally connect parcels, b_{nv} are the parameters for distance interaction Δt_n is the time delay calculated in the connectivity matrix step. ε_n is white noise (ATR Neural Information Analysis Labs, n.d.-b; Runfeng, 2018).

Movie Creation

Input: Mar model, parcel currents, parameters (time window, sampling rate), fiber tracking input

Output: parcel current movie

In this step, a movie is created from the estimated dynamics. The movie displays the estimated parcel currents and connectome dynamics in a clear overview. Fiber tracking is performed again on a subset of data to obtain fiber shapes to display connections. In the next step, the movie is created using the create_movie function from the VBMEG toolbox. The movie displays the source currents of one node with its own contribution (local dynamics), the contribution from other parcels and, contribution from input (ATR Neural Information Analysis Labs, n.d.-a).

Appendix B: VBMEG installation

The current chapter describes the system deployment of the VBMEG toolbox. The VBMEG requires several programs to run:

- Matlab (version 2021 is compatible), from: https://nl.mathworks.com/products/new_products/latest_features.html
- Freesurfer (version 7 is compatible), available from: https://surfer.nmr.mgh.harvard.edu/
- FSL (v6.0), available from: https://fsl.fmrib.ox.ac.uk/fsl/fslwiki/
- MRtrix (v 0.2.13, MRtrix3 **not** compatible) available from: https://www.nitrc.org/frs/?group_id=128
- (optional) EEGLAB available from: https://eeglab.org/

An installation script was made for the VBMEG toolbox using a bash shell script. The script has two options, a fast install, and a manual install. The fast install installs all programs automatically in one go. The manual install is more hands-on and asks which programs are to be installed.

The user has to set a couple of different variables:

- Download directory: directory where all programs are downloaded to
- Program directory: directory where all programs should be installed in
- LOG directory: directory to save installation logs
- Matlab directory: directory to save Matlab scripts and data

The user must have root privileges to install most programs, so the installation should be run as a root user. If not, the script is terminated.

First, all required dependencies are installed. Then, all programs are then installed in order. Some errors exist in the VBMEG toolbox. The script corrects those errors using the -sed command from Linux.

- The VBMEG requires and VBMEGrc file to find the correct paths to all installed programs. This file is edited with the correct paths.
- The function dmri_fs_info read is edited to convert .gii files into .asc files. Otherwise, the VBMEG toolbox cannot load the files properly.
- The rename package by Linux has been updated and works differently. VBMEG uses the old convention. The installation script updates the VBMEG scripts use the new package.

- The FSL viewer the VBMEG toolbox uses has been changed. In order to use the same viewer, FSLview must be changed to fslview_deprecated in 8 of the VBMEG files. A new viewer called FSL eyes is also available but is not implemented.

Future Improvements

The installation script still has room for improvement for the VBMEG toolbox to work out of the box. Some suggestions are:

- Add option for the user to auto edit the VBMEG toolbox to run fiber tracking on the localhost. Recently was discovered that fiber tracking can be performed on the localhost without setting up the ssh connection to localhost as explained in: https://vbmeg.atr.jp/docs/v22/attachFile/vbmeg_users_manual/dmri_data_processing_en.pdf. Automating this step would make installation less cumbersome.
- MRTrix has an updated version with different commands. Existing MRTrix commands can be updated to be compatible with a new version of MRTrix.
- The FSL viewer can be updated to work with FSL eyes.
- Currently, the script only functions for Linux computers. A windows option can be created.